

Diffuse Molecular Cloud Densities from UV Measurements of CO Absorption

Paul F. Goldsmith

Jet Propulsion Laboratory, California Institute of Technology

Received _____; accepted _____

arXiv:1307.8374v1 [astro-ph.GA] 31 Jul 2013

1. Abstract

We use UV measurements of interstellar CO towards nearby stars to calculate the density in the diffuse molecular clouds containing the molecules responsible for the observed absorption. Chemical models and recent calculations of the excitation rate coefficients indicate that the regions in which CO is found have hydrogen predominantly in molecular form. We carry out statistical equilibrium calculations using CO–H₂ collision rates to solve for the H₂ density in the observed sources without including effects of radiative trapping. We have assumed kinetic temperatures of 50 K and 100 K, finding this choice to make relatively little difference to the lowest transition. For the sources having T_{10}^{ex} only, for which we could determine upper and lower density limits, we find $\langle n(H_2) \rangle = 49 \text{ cm}^{-3}$. While we can find a consistent density range for a good fraction of the sources having either two or three values of the excitation temperature, there is a suggestion that the higher- J transitions are sampling clouds or regions within diffuse molecular cloud material that have higher densities than the material sampled by the $J = 1-0$ transition. The assumed kinetic temperature and derived H₂ density are anticorrelated when the $J = 2-1$ transition data, the $J = 3-2$ transition data, or both are included. For sources with either two or three values of the excitation temperature, we find average values of the midpoint of the density range that is consistent with all of the observations equal to 68 cm^{-3} for $T^k = 100 \text{ K}$ and 92 cm^{-3} for $T^k = 50 \text{ K}$. The data for this set of sources imply that diffuse molecular clouds are characterized by an average thermal pressure between 4600 and 6800 Kcm^{-3} .

Keywords: ISM: molecules - radio lines: ISM

2. Introduction

Diffuse clouds have been studied over a broad range of wavelengths encompassing radio observations of the 21 cm H I line to UV observations of H₂ and other molecules. They have been found to encompass a wide range of densities, temperatures, and column densities. For low column densities, the gas is essentially atomic (H⁰) and ionic (C⁺), but as the column density and extinction increase, molecules (starting with H₂) gradually become dominant, and the term “diffuse molecular cloud” (Snow & McCall 2006) is appropriate. Ground-based observations of strong millimeter continuum sources (Liszt & Lucas 1998) and UV observations of early-type stars (e.g. Sheffer et al. 2008) have both allowed observations of rotational transitions of the CO molecule. The UV observations are particularly powerful in that they allow simultaneous measurements of multiple transitions, which are sensitive to the column density of the different CO rotational levels in the cloud in the foreground of the star. The column density of H₂ can also be determined, which allowing determination of the abundances of a number of different species and also isotope ratios as a function of column density (Sheffer et al. 2007).

The density of diffuse molecular clouds is an important parameter for analyzing emission in various tracers as well as determining a number of critical cloud properties such as their thermal pressure. One important tracer of several phases of the interstellar medium including diffuse clouds is the fine structure transition of ionized carbon ([C II]). Several groups using the Herschel Satellite (Pilbratt et al. 2010) have carried out extensive observations of this submillimeter ($\lambda = 158 \mu\text{m}$) transition. Among these, a large-scale survey of the Milky Way has been attempting to apportion the observed [CII] emission among the different phases of the interstellar medium (Langer et al. 2010; Pineda et al. 2013). The [C II] emission from the diffuse cloud component of the interstellar medium will almost certainly be subthermal given that the critical density for the [C II] fine structure

line is $\simeq 2000 - 6000 \text{ cm}^{-3}$ (Goldsmith et al. 2012). Since the [C II] transition is optically thin or in the effectively optically thin limit (Goldsmith et al. 2012), the inferred column density of ionized carbon in the diffuse interstellar medium will vary inversely as the density in the clouds responsible for the [C II] emission. The cooling and thermal balance are also sensitively dependent on the density, so that understanding the structure of diffuse clouds and their role in the formation of denser clouds and star formation requires knowledge of the density in the diffuse interstellar medium.

In this paper we use the relative populations of the lower CO rotational levels to determine the density in the diffuse clouds along the line of sight to early-type stars observed in the UV. Data on sixty four sources were taken from Sheffer et al. (2008). We have supplemented these data with observational results on eight distinct sources observed by Sonnentrucker et al. (2007), who also present data obtained by Lambert et al. (1994) and Federman et al. (2003) for three sources. Two additional, distinct sources were observed by Burgh, France, & McCandliss (2007).

In Section 3 we discuss the transformation of the Sheffer et al. (2008) data to standard excitation temperatures that characterize successive rotational transitions, and in Section 4 derive the uncertainties in the excitation temperatures resulting from their column density measurements. In section 5 we discuss the possibility of radiative excitation, and conclude that it is unlikely to play a significant role. We focus on collisional excitation of CO, concluding that collisions with H₂ molecules are dominant in the clouds of interest. Section 6 gives the results for different categories of diffuse clouds defined by which CO transitions have been observed. In Section 7 we discuss and summarize our results. The Appendix gives an explanation of long-standing apparently anomalous results for the excitation temperature in the low-density limit from multilevel statistical equilibrium calculations that can, in fact, be understood in terms of the allowed collisions and the spontaneous

decay rates.

3. Excitation Temperatures

The excitation temperature, T^{ex} , is defined by the relative local densities in two different energy levels, or (having a clear physical meaning if conditions are uniform along the line of sight) by the relative column densities, N , of the two levels of a given species. Denoting the upper and lower levels by u and l , respectively, and their statistical weights by g_u and g_l , the relationship is

$$\frac{N_u}{N_l} = \frac{g_u}{g_l} \exp[-\Delta E_{ul}/kT_{ul}^{ex}] , \quad (1)$$

where ΔE_{ul} is the energy difference between the upper and the lower level. The excitation temperature can be defined between any pair of levels, but it is of greatest utility for two levels connected by a radiative transition that can be observed.

Sheffer et al. (2008) use UV absorption measurements to determine the column densities in a number of the lowest transitions of the carbon monoxide (CO) molecule, and define the excitation temperatures of the excited rotational levels ($J = 1, 2, 3$) relative to the ground state, $J = 0$. The lowest excitation temperature thus defined corresponds to the CO $J = 1 - 0$ transition at 115.3 GHz. The excitation temperatures related to column densities of the $J = 2$ and $J = 3$ levels relative to $J = 0$ do not correspond to observable transitions. It is convenient for density determinations to deal with pairs of levels connected by a radiative transition, so that the collision rate directly competes with an allowed radiative processes. The results tabulated by Sheffer et al. (2008) can easily be transformed into the desired excitation temperatures through the following relationships, in which T_{01} , T_{02} , and T_{03} are the excitation temperatures of the indicated pairs of levels determined by Sheffer et al. (2008), and T_{01}^{ex} , T_{21}^{ex} , and T_{32}^{ex} are the excitation temperatures

for radiatively-connected pairs of levels. We define for each transition the equivalent temperature, $T_{ul}^* = \Delta E_{ul}/k$,

$$T_{10}^{ex} = T_{01} \quad (2)$$

$$T_{21}^{ex} = T_{21}^* \frac{T_{02}T_{01}}{T_{20}^*T_{01} - T_{10}^*T_{02}} \quad (3)$$

$$T_{32}^{ex} = T_{32}^* \frac{T_{03}T_{02}}{T_{30}^*T_{02} - T_{20}^*T_{03}} . \quad (4)$$

The transformed results for the stars observed by Sheffer et al. (2008) are given in Table 1, along with the molecular hydrogen column density determined for each line of sight. In two cases, the H₂ column density was estimated by Sheffer et al. (2008) from the column densities of CO and CH, and these values are singled out by a note in the Table. For four lines of sight, Sheffer et al. (2008) did not include N(H₂), but values for these were found in the literature and values with associated references are given in column 5 of Table 1. The data in Table 6 of Lambert et al. (1994), Table 1 of Burgh, France, & McCandliss (2007), and Table 12 of Sonnentrucker et al. (2007) are presented in the form of excitation temperatures between adjacent rotational levels and so can be used directly. These data are presented in Table 2, along with references to the original observational papers.

4. Uncertainties

In deriving excitation temperatures, T_{ex} from column densities N , we use the usual relationship given in equation 1, which leads to the expression for the excitation temperature

$$T^{ex} = \frac{T^*}{\ln\left[\frac{N_l g_u}{N_u g_l}\right]} . \quad (5)$$

Taking the partial derivatives with respect to upper and lower level column densities,

we find

$$\frac{dT^{ex}}{T^{ex}} = \frac{T^{ex}}{T^*} \left[\frac{dN_l}{N_l} - \frac{dN_u}{N_u} \right] . \quad (6)$$

Defining the rms uncertainties as $\sigma_{T^{ex}}$, σ_{N_l} , and σ_{N_u} , respectively, and combining the fractional uncertainties as the sum of the squared uncertainties in the lower and upper level column densities gives us

$$\frac{\sigma_{T^{ex}}}{T^{ex}} = \frac{T^{ex}}{T^*} \left[\left(\frac{\sigma_{N_l}}{N_l} \right)^2 + \left(\frac{\sigma_{N_u}}{N_u} \right)^2 \right]^{0.5} . \quad (7)$$

For the UV absorption data of interest, the excitation temperatures are on the order of 0.6 to 0.8 times T^* (e.g. 4 K for the $J = 1-0$ transition having $T^* = 5.5$ K). It is thus reasonable to take $T^{ex}/T^* \simeq 0.7$, which gives us

$$\frac{\sigma_{T^{ex}}}{T^{ex}} = 0.7 \left[\left(\frac{\sigma_{N_l}}{N_l} \right)^2 + \left(\frac{\sigma_{N_u}}{N_u} \right)^2 \right]^{0.5} . \quad (8)$$

Sheffer et al. (2008) give only the uncertainty in the total column density of CO. While it is not clear exactly how the uncertainty in the total column density is related to the fractional uncertainty in the column density of a single level, we simply assume that the fractional uncertainty in an individual column density is equal to the total CO column density uncertainty, given as 20% by Sheffer et al. (2008). Then the fractional uncertainty in the excitation temperature is $\simeq 0.7\sqrt{2}$ times 20%. It thus seems that a reasonably generous 1σ value is $\sigma_{T^{ex}}/T^{ex} = 0.2$.

The observations taken from other papers (Table 2) explicitly include uncertainties in individual excitation temperatures. As seen in that Table, these vary considerably from source to source, but are of the same order as given by the above analysis.

5. CO Excitation

5.1. Non-Collisional Excitation

The excitation of CO can, in principle, be affected by radiative processes following its formation. The unshielded photodissociation rate of ^{12}CO in a radiation field having the standard Draine value (Draine 1978) is $k_{i0} = 2 \times 10^{-10} \text{ s}^{-1}$ (UMIST 2012). For the H_2 and CO column densities of the clouds in this sample, the shielding factor is $\simeq 0.5$ (see Van Dishoeck & Black 1988, Table 5), and thus the CO photodissociation rate within the cloud, which we take equal to the formation rate, is on the order of 10^{-10} s^{-1} . The characteristic time scale is thus $\simeq 300 \text{ yr}$. The vibrational decay rate is enormously faster, with $A(v = 1 - v = 0) = 30.6 \text{ s}^{-1}$ (Chandra, Maheshwari, & Sharma 1996). Thus, any CO molecule formed will very rapidly decay to the ground vibrational state. The spontaneous decay rates for the rotational transitions are many orders of magnitude slower, ranging from $A_{10} = 7.2 \times 10^{-8} \text{ s}^{-1}$ to $A_{32} = 2.5 \times 10^{-6} \text{ s}^{-1}$ for the transitions considered here (CDMS).

The collision rates necessary to achieve the observed subthermal excitation of CO (see Section 6) are $\simeq 10^{-8} \text{ s}^{-1}$ or 100 times the formation timescale. Thus with all CO molecules being in the ground vibrational state, the collision rate that determines the rotational level populations will be much more rapid than formation/destruction rate, and it is reasonable that the effect of a post-formation cascade (as can affect the population of the levels of H_2) will be unimportant.

Wannier et al. (1997) suggested that the radiation from a nearby, dense molecular cloud could be sufficient to provide the observed excitation of CO in a diffuse molecular cloud. This requires that the two clouds have the same velocity and that the solid angle of the cloud providing the radiative pumping be large enough to make the radiative excitation rate comparable to the spontaneous decay rate of the transition observed. Sonnentrucker

et al. (2007) pointed out that a critical test of this model follows from the fact that the pumping cloud, while optically thick in ^{12}CO would almost certainly be optically thin in ^{13}CO . The result would be a much lower radiative pumping rate for ^{13}CO than for ^{12}CO , and the excitation temperatures of the rare isotopologue would thus be significantly smaller. Sonnentrucker et al. (2007) conclude that for 7 sight lines (including some observed by others) $T_{10}^{ex}(^{12}\text{CO})$ is, within the uncertainties, equal to that of ^{13}CO .

An additional consideration is that the excitation temperature $T_{J,J-1}^{ex}(^{12}\text{CO})$ increases with increasing J ; this increase is predicted by the collisional excitation model discussed in the Appendix. For ^{13}CO , there are only two sources with excitation temperatures determined for more than one transition. Both of these, HD147933 (Lambert et al. 1994) and HD24534 (Sonnentrucker et al. 2007), show this behavior. Given the constraints imposed by the limited signal to noise ratio, it is difficult to be definitive, but we agree with Sonnentrucker et al. (2007) that radiative excitation by nearby clouds does not play a major role in determining the excitation temperature of the lower rotational transitions of CO and that excitation is primarily by collisions. Zsargó & Federman (2003) similarly concluded that optical pumping is generally unimportant for excitation of CI in diffuse clouds.

5.2. Collisional Excitation of CO in Diffuse Molecular Clouds

Analyzing the excitation of CO and determining the density of diffuse clouds is linked to their structure. Possibly important collision partners in diffuse clouds are electrons, atomic hydrogen (H^0) and molecular hydrogen (H_2). In these clouds, carbon is largely in ionized form (see, for example Figure 1) so the fractional abundance of electrons $\simeq 10^{-4}$ throughout diffuse molecular clouds. Crawford & Dalgarno (1971) calculated the cross sections for excitation of low- J transitions of CO due to collisions with electrons.

Their results are reproduced by the general, but more approximate treatment of Dickinson & Richards (1975), who calculate excitation rate coefficients and fit a quite convenient general formula. Application to the low-dipole moment CO molecule, yields characteristic deexcitation rate coefficients between 0.4 and $0.5 \times 10^{-8} \text{ cm}^3\text{s}^{-1}$, for kinetic temperatures between 50 K and 150 K, and for J_{upper} between 1 and 6. These are approximately a factor of 100 larger than those for collisions with atomic or molecular hydrogen (see discussion in Section 5.5).

However, this is not a sufficient factor to compensate for the much lower fractional abundance of electrons, and in consequence electrons should not be a significant source of collisional excitation for CO in diffuse clouds. The more detailed discussion in Section 5.5 thus considers only excitation by collisions with H^0 and H_2 . Note that this situation is quite different than that for high-dipole moment molecules such as HCN (Dickinson et al. 1977), since the coefficients for electron excitation scale approximately as μ^2 . Thus for HCN or CN, electron excitation rate coefficients will be 10^4 to 10^5 times larger than those for collisions with atoms or molecules.

5.3. Cloud Structure, the H^0 to H_2 Transition, and Excitation Analysis

We are left with atomic and molecular hydrogen as being significant for collisional excitation of CO in diffuse molecular clouds. The distribution and abundance of each varies through a cloud due to the competition between formation and photodissociation; the latter is mediated by self-shielding. The processes determining the transformation between H^0 and H_2 are well-treated by the Meudon PDR code (Le Petit et al. 2006). We have carried out a number of runs modeling slabs exposed to the interstellar radiation field on both sides, with a uniform density defined by $n(\text{H}) = n(\text{H}^0) + 2n(\text{H}_2)$. The critical results are summarized in Table 3. We include the molecular fraction defined by $f(\text{H}_2) =$

$2n(\text{H}_2)/(2n(\text{H}_2) + n(\text{H}^0))$, defined in the central portion of the cloud, and also integrated through the entire cloud, which we denote $F(\text{H}_2)$ following Snow & McCall (2006). For clouds having extinction exceeding a few tenths of a magnitude, a large fraction of hydrogen is in molecular form. What is particularly important to note is that the H_2 fraction in the centers of the slab is high, generally ≥ 0.75 , and in some relevant cases, > 0.9 .

From the data on color excess presented by Rachford et al. (2002) and Sheffer et al. (2008) we can determine the total hydrogen column density $N(\text{H})$ and the integrated hydrogen fraction for some of the sources observed here. The values for most sources are $\simeq 0.5$, confirming that, for the sources here, a large fraction of the hydrogen will be in molecular form. This is consistent with the information presented in Table 2 of Burgh, France, & McCandliss (2007) showing that $F(\text{H}_2) \geq 0.24$ for 8 of the 9 sources with $N(\text{H}_2) > 10^{20} \text{ cm}^{-2}$. The one exception, HD102065, has a reasonable density range determined with a single CO transition (Table 4), but an enhanced UV field could result in the low integrated molecular fraction, $F(\text{H}_2) = 0.1$ (Burgh, France, & McCandliss 2007). $F(\text{H}_2)$ is not obviously correlated with $N(\text{H})$, suggesting that other characteristics such as cloud density and environment play an important role in determining the balance between atomic and molecular hydrogen.

This situation is illustrated by the cloud model results shown in Figure 1. The H_2 density exceeds that of H^0 for visual extinctions ≥ 0.03 mag, and in the central region of the cloud, $n(\text{H}_2) \simeq 50 \text{ cm}^{-3}$, which is quite similar to the average value determined below in Section 6. The kinetic temperature varies between $\simeq 50 \text{ K}$ and $\simeq 100 \text{ K}$ throughout the cloud, also in good agreement with observations (e.g. Table 6 of Sheffer et al. 2008). While this treatment does not consider all combinations of extreme conditions, it is reasonable to conclude that diffuse molecular clouds have a largely molecular hydrogen core, surrounded by a region in which the hydrogen is primarily atomic. The size of the molecular core, the

peak H_2 fraction, and the integrated H_2 fraction all increase with increasing cloud density, and decrease as the strength of the interstellar radiation field increases. It is thus plausible that in diffuse clouds with visual extinction of a few tenths to $\simeq 1$ mag, such as most of those observed in the above-cited papers, the density of H_2 is a factor 2 to 10 times larger than that of H^0 . This is consistent with the properties suggested for “transitional clouds” studied in HI self-absorption by Kavars et al. (2005).

A consideration when comparing these models with observations is the question of multiple clouds along the line of sight. Welty & Hobbs (2001) find that their extremely high spectral resolution (ground-based) observations require multiple, relatively narrow velocity components in order to obtain good fits to their observed KI line profiles. Such resolution is not available for UV observations of CO, but the observed cloud parameters may, in fact, refer to the sum of a number of individual components.

The major effect of multiple clouds is that the extinction in each individual component cloud is smaller than the total line of sight extinction. The clouds being considered here have (measured) H_2 column densities between 1 and $6 \times 10^{20} \text{ cm}^{-2}$. This alone corresponds to extinctions between 0.1 and 0.6 mag. If we assume a nominal integrated H_2 fraction $F(\text{H}_2) = 0.6$, $N(\text{H}^0) = 1.33N(\text{H}_2)$, and the atomic hydrogen column density envelope raises the total extinction through the cloud to $\simeq 0.2 - 1.0$ mag. If we have, for example, three equal component clouds along the line of sight, each has extinction between 0.07 and 0.33 mag. In conditions of standard radiation field intensity and $n(\text{H}) \geq 100 \text{ cm}^{-3}$, the peak H_2 fraction will reach 0.5 for the lowest column density clouds, and will be close to unity for those having the highest column densities. Thus, even the presence of a modest number of components along the line of sight will not change the basic picture of a constituent cloud having a primarily molecular H_2 core surrounded by a H^0 envelope.

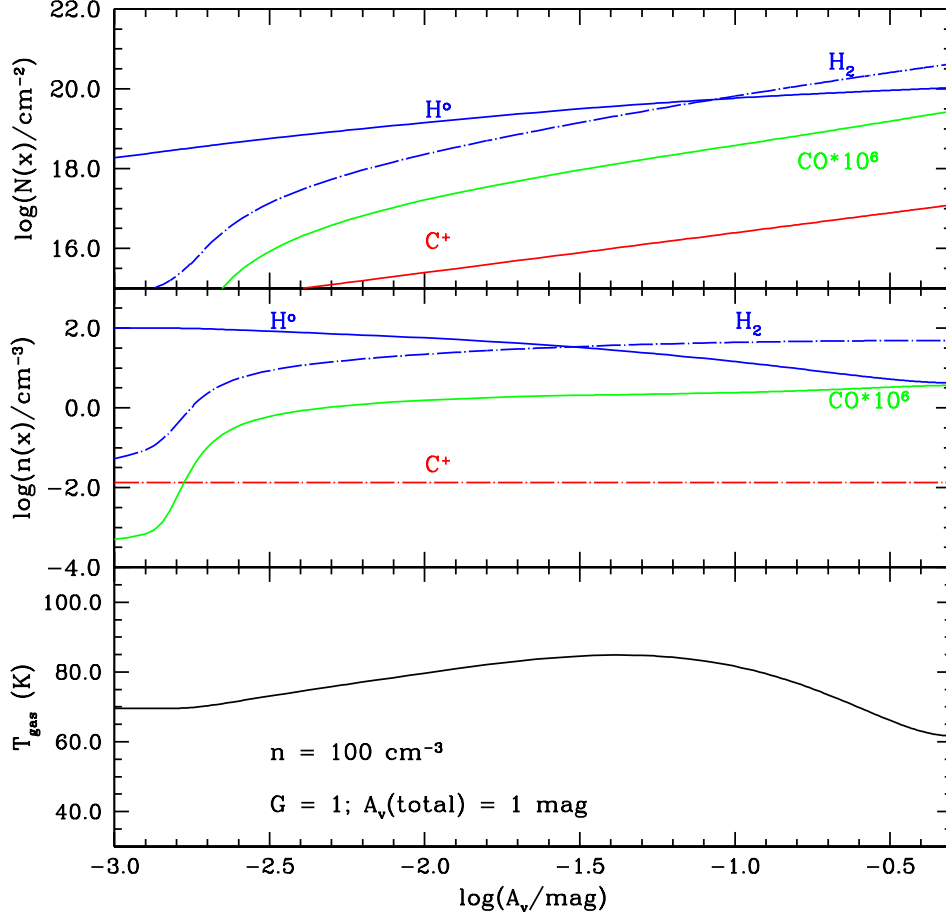


Fig. 1.— Results of model calculation using the Meudon PDR code for a two-sided slab exposed on both sides to an interstellar radiation field of standard intensity. The proton density $n(\text{H})$ is equal to 100 cm^{-3} . The bottom panel shows the variation of the kinetic temperature through the cloud. The middle panel shows the volume densities of ionized carbon, CO, H^0 , and H_2 . Note that the H_2 density in the central portion of the cloud is close to 50 cm^{-3} . The upper panel shows the column densities of these four species integrated from the edge of the cloud.

5.4. CO Chemistry

Another factor is the chemistry of CO. While it is not appropriate to go into this in much detail here, a short review is important to appreciate where in the observed clouds the CO being observed is actually located. In clouds where hydrogen is atomic, the only route to form CO starts with the radiative association reaction of C^+ and H^0 . This reaction is extremely slow, but the CH^+ that forms yields (through reaction with O) a slow rate of CO production, and combined with relatively unattenuated photodissociation, results in a low fractional abundance of CO. In clouds with the hydrogen in the form of H_2 , a similar radiative association reaction between C^+ (which will still be the dominant form of carbon due to its lower ionization potential) and H_2 can take place, but it is $\simeq 40$ times faster than that with H^0 , leading to somewhat higher CO fractional abundances. A second path is the chemical reaction $C^+ + H_2 \rightarrow CH^+ + H$. However, this reaction is endothermic by 4640 K, and thus is extremely slow at normal cloud temperatures. The above pathways lead to a fractional abundance of CO in diffuse molecular regions $\simeq 3 \times 10^{-8}$, similar to that seen in Figure 1, but significantly below that observed for diffuse molecular clouds being considered here ($\langle N(CO)/N(H_2) \rangle = 3 \times 10^{-7}$; Federman et al. (1980), Sheffer et al. (2008)).

Elitzur & Watson (1978) suggested that presence of shock heating would significantly raise the temperature of the molecular gas and enhance the abundance of CH^+ . This would also have the effect of increasing the abundance of CO. This could resolve the discrepancy between model and observations, but has the undesirable consequence of copiously producing OH via the reaction $O + H_2 \rightarrow OH + H$, which is endothermic by 3260 K. The predicted OH fractional abundance exceeds that observed by a large factor.

In order to exploit the rapid reaction between C^+ and H_2 at high temperatures without overproducing OH, Federman et al. (1996) suggested that Alfvén waves could heat diffuse clouds and the outer portions of larger molecular clouds with the special effect of raising the

temperature of the ions and not that of the neutrals. Thus, CH^+ , and CO abundances could be enhanced without overproducing OH. This "superthermal" chemistry was supported by observations of various species by Zsargó & Federman (2003) and has subsequently been incorporated into different models, notably that of Visser, van Dishoeck, & Black (2009), that successfully reproduce the run of CO *vs* H_2 column densities.

An alternative explanation that explains the abundances of a number of species in diffuse molecular clouds is heating in regions of turbulent dissipation, discussed by Godard, Falgarone, & Pineau des Forêts (2009). What is essential for the present discussion is that these models are entirely dependent on having molecular hydrogen as the starting point. In contrast, no models starting with atomic hydrogen can achieve fractional abundances of CO close to those observed. Thus, the chemistry of CO strongly suggests that we are tracing a species confined to the portion of the cloud in which hydrogen is largely in the form of H_2 . Note that the Meudon PDR code does not include superthermal chemistry so that the CO fractional abundances predicted (e.g. Figure 1) are significantly below those derived from observations.

5.5. Collision Rate Coefficients

Due to the importance of CO in the dense interstellar medium in which hydrogen is almost entirely molecular, cross sections and excitation rates for collisions between CO and H_2 have been calculated by several different groups starting more than three decades ago (Green & Thaddeus 1976; Flower 2001; Wernli et al. 2006; Yang et al. 2010). The earliest calculations treated H_2 molecules as He atoms (with a simple scaling for their different mass), which is correct only for the lowest, spherically symmetric level ($J = 0$) of para- H_2 . This calculation is thus strictly speaking not applicable to ortho- H_2 , which is expected to have comparable or even greater abundance than the para- H_2 spin modification. While the

details of the potential surfaces and the quantum calculations have evolved, the results are all quite similar. Figure 2 includes the more detailed calculations that treat ortho-H₂ and para-H₂ as separate species. As seen in Figure 2, there is very little difference between the deexcitation rate coefficients for ortho- and for para- H₂.

To model the excitation of CO by collisions with H₂ in diffuse clouds, we use the most recent results of Yang et al. (2010) as given in the LAMDA database. We have adopted an ortho-to-para H₂ ratio (OPR) equal to 3, but varying the OPR from 1 to 3 does not make a significant difference in the excitation temperature for a given total H₂ density. The results for the three lowest CO transitions for three kinetic temperatures representative of the temperatures measured for this sample of diffuse molecular cloud sight lines are shown in Figure 3. We see that the excitation temperatures of all three transitions increase monotonically with the H₂ density throughout this range. For densities below $\simeq 50 \text{ cm}^{-3}$, the excitation temperatures T_{JJ-1}^{ex} increase as J increases. This apparently surprising behavior is discussed in detail in the Appendix. All transitions are assumed to be optically thin for these calculations.

The situation for collisions between hydrogen atoms and CO molecules is less satisfactory. H⁰-CO collisions were analyzed by Chu & Dalgarno (1975), who found cross sections for H⁰-CO collisions comparable to those for H₂-CO collisions for small ΔJ which are numerically the largest. Green & Thaddeus (1976) carried out calculations for H⁰ colliding with CO, with quite different results. First, the magnitude of the collision rate coefficients are an order of magnitude smaller ($1\text{--}2 \times 10^{-11} \text{ cm}^3\text{s}^{-1}$ compared to $10^{-10} \text{ cm}^3\text{s}^{-1}$). Second, the Green & Thaddeus (1976) rate coefficients are very small for $|\Delta J| \geq 3$ compared to those for $|\Delta J| = 1$ or 2. A more recent calculation (Balakrishnan, Yan, & Dalgarno 2002) suggested cross sections for H⁰-CO collisions a factor $\simeq 25$ larger in total magnitude (compared to Green & Thaddeus (1976)), and with large- ΔJ transitions

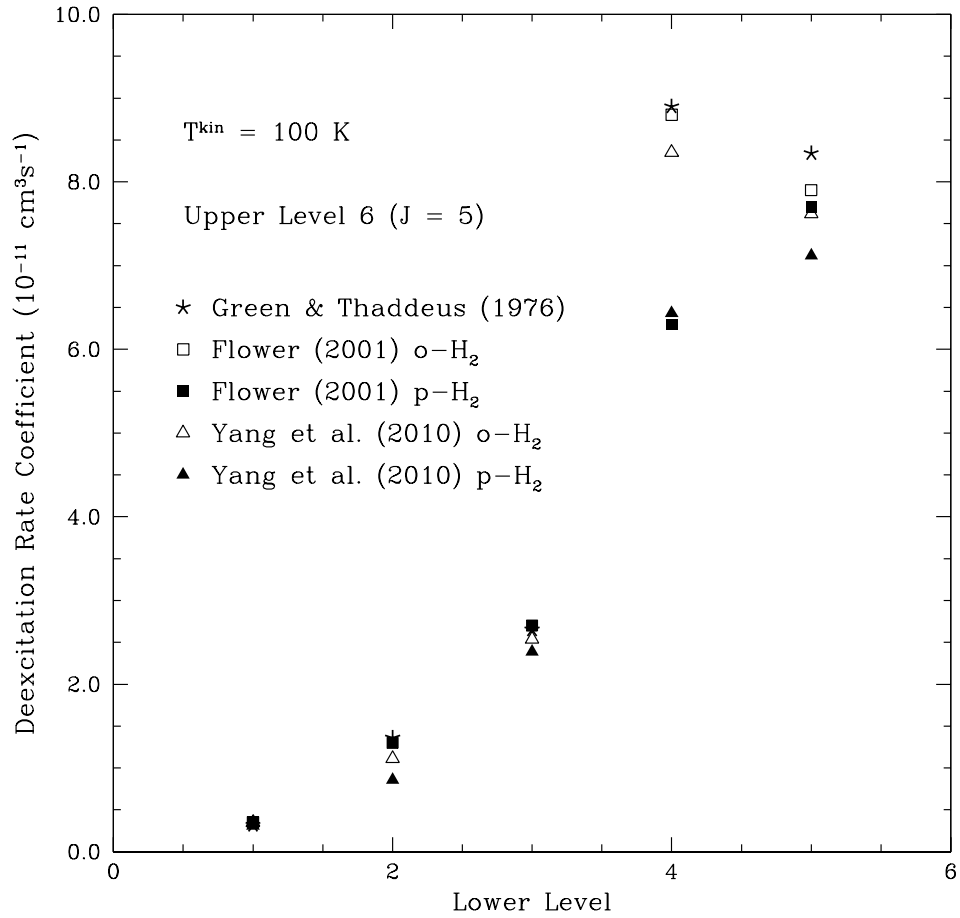


Fig. 2.— Comparison of different calculations of the CO deexcitation rate coefficients for collisions with H₂. This limited sample, which includes only initial level 6 ($J = 5$) transitions to lower levels, indicates agreement to within $\pm 20\%$.

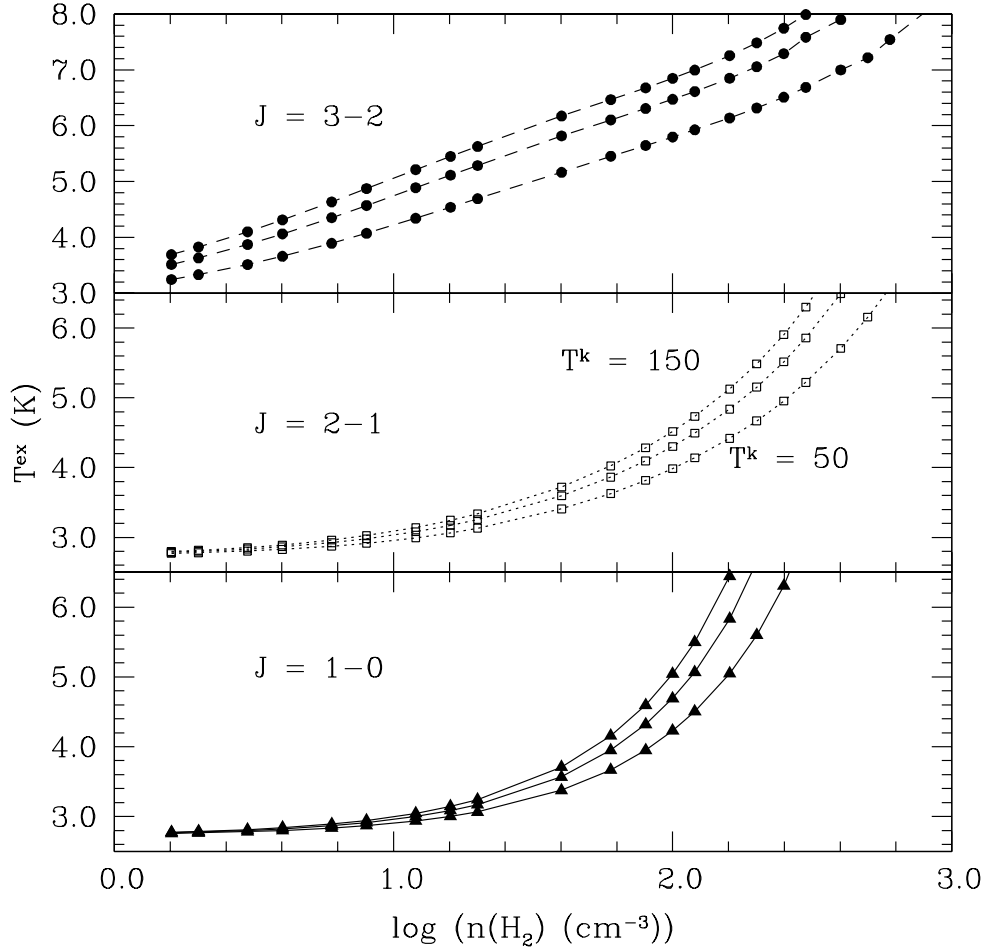


Fig. 3.— Excitation temperatures for the three lowest transitions of CO as function of H_2 density for three kinetic temperatures representative of this sample of lines of sight through diffuse clouds. All transitions are assumed to be optically thin. The curves for each rotational transition are for kinetic temperatures $T^k = 150$ K, 100 K, and 50 K, from left to right. An ortho-to-para ratio (OPR) equal to 3 has been assumed in all cases. The collision rate coefficients are those of Yang et al. (2010).

enhanced by up to 1000. However, a subsequent reconsideration by Shepler et al. (2007) of the interaction potential employed suggested that the results of Balakrishnan, Yan, & Dalgarno (2002) are erroneous¹. This is confirmed by a very recent paper by Yang et al. (2013), which finds results for H⁰–CO collisions very similar to those of Green & Thaddeus (1976).

In Figure 4 we compare the excitation temperatures of the three lowest CO rotational transitions produced by collisions with H⁰ and H₂ (based on the Green & Thaddeus (1976) rate coefficients for collisions with H⁰ and the Yang et al. (2010) rate coefficients for collisions with H₂). The form of the excitation temperature curves are the same for both types of colliders, but shifted by a factor of $\simeq 5$ for the two lowest transitions and a factor $\simeq 25$ for the $J = 3-2$ transition. The relative ordering of the T^{ex} is highly sensitive to the density of colliding particles. One contributor to this is the fact that the $J = 1-0$ transition is heading towards a population inversion with equal upper and lower level populations and resulting infinite excitation temperature. From this we see that for H₂ fraction $f(\text{H}_2) \geq 0.3$, collisions with H₂ will be dominant, and for $f(\text{H}_2) \geq 0.5$, the H⁰ is unimportant for collisional excitation.

Based on the modeling of diffuse molecular clouds in terms of the distribution of H₂ and H⁰ as a function of optical depth, the CO chemistry, and the relative magnitudes of the collision rate coefficients for collisions with H₂ and H⁰ as well as the lack of convincing evidence for any non-collisional excitation mechanism, it appears very likely that collisions with H₂ molecules are the dominant source of collisional excitation of CO molecules. Consequently, from the observed excitation temperatures we should be able to derive the H₂ density in diffuse molecular clouds. Any result is, of course, subject to the caveat of being

¹We are indebted to Dr. Balakrishnan for a private communication on this subject advising use of the Green & Thaddeus (1976) calculations for H⁰–CO collisions.

an average of the regions with CO along the line of the sight, including multiple clouds, if present.

6. Density Determination

We divide the analysis into two parts. The first is for the sources for which there is only data for the lowest transition. For these sources with only a single value of the excitation temperature to fit, we can determine an upper limit to the density or a range of densities, depending on the value of T_{10}^{ex} . The second part is for sources with multiple transitions, for which we must also consider the consistency between the results from the different transitions observed. For the Sheffer et al. (2008) data, we consider the uncertainty in the value of T^{ex} to be that given in Section 4, namely $\sigma_{T^{ex}}/T^{ex} = 0.2$, while for the other data we use the uncertainties provided.

6.1. Optical Depth

The optical depth of the $J = 1-0$ CO transition can be written

$$\tau(1, 0) = 3.0 \times 10^{-4} \left(\frac{N_{12}}{\delta v_{kms}} \right) (e^{5.53/T_{10}^{ex}} - 1) f_{J=1} , \quad (9)$$

where N_{12} is the column density of CO in units of 10^{12} cm^{-2} , δv_{kms} is the FWHM line width in kms^{-1} , and $f_{J=1}$ is the fraction of the molecules in the upper ($J = 1$) state. Under the subthermal conditions encountered here, it is not correct to assume that all transitions have the same excitation temperature or to adopt the usual expression for the partition function, $Q = KT/hB_0$. The higher- J transitions have lower optical depths for the densities in the range of interest for these diffuse molecular clouds. The excitation-dependent terms in the above equation vary among the clouds studied here, but their product is not far from unity. While the lines are not spectrally resolved, high-resolution ground-based observations of

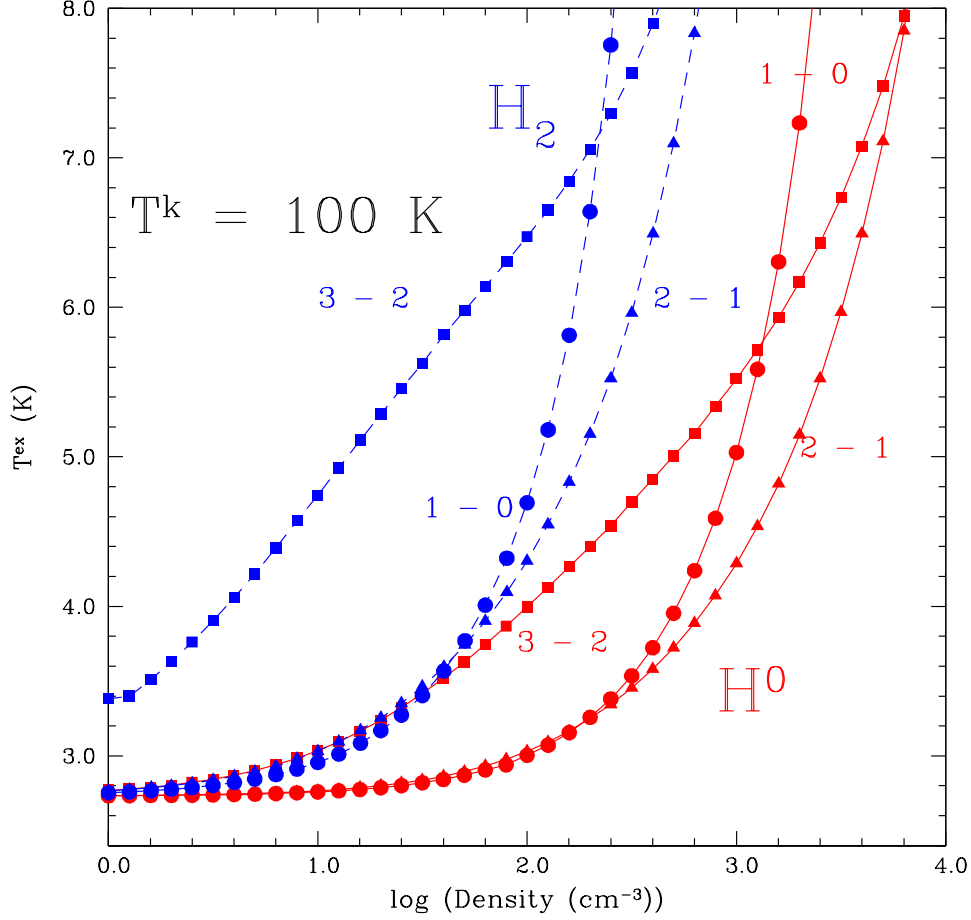


Fig. 4.— Excitation temperature of the three lowest rotational transitions of CO as a function of colliding particle density. The kinetic temperature is 100 K and all CO transitions are optically thin. The $J = 3-2$ transition is denoted by the squares, the $J = 2-1$ transition by triangles, and the $J = 1-0$ transition by circles. The two sets of transitions correspond to collisions with H_2 (broken lines) and with H^0 (solid lines). A factor $\simeq 10$ higher $n(\text{H}^0)$ than $n(\text{H}_2)$ is required to produce the same value of T_{10}^{ex} or T_{21}^{ex} while a factor $\simeq 25$ higher H^0 than H_2 density is required to produce equal values of T_{32}^{ex} .

species such as CH and CH⁺ as templates suggest FWHM line widths $\simeq 3 \text{ km s}^{-1}$. Thus, $\tau(1,0) \simeq 10^{-4}N_{12}$. Even if the entire line of sight CO column density is incorporated into a single cloud, the optical depth for almost all clouds included here is considerably less than unity, with the highest column density cloud (having $N_{12} = 10^4$) just reaching this limit. If the column density is divided among several clouds that each subtends only a small solid angle as seen by the others, the radiative trapping will be reduced accordingly. We thus do not consider trapping to be a significant contributor to the CO excitation for the clouds considered here, although this will not be the case, for example, for translucent clouds with larger CO column densities.

6.2. Kinetic Temperatures

The kinetic temperature shows considerable variation among diffuse molecular clouds. Savage et al. (1977) employed UV observations of H₂ in the $J = 0$ and $J = 1$ rotational levels, and with the assumption that the relative population of these ground rotational levels of para- and ortho-H₂ reflects the kinetic temperature, found that clouds with $N(\text{H}_2)$ greater than 10^{18} cm^{-2} have kinetic temperatures between 45 and 128 K, with an average values for 61 stars of 77 ± 17 (rms) K. Rachford et al. (2002) used a similar technique, finding a slightly lower mean value, with $\langle T^k \rangle = 68 \text{ K}$, and a variance of 15 K, although there were three lines of sight having $T^k > 94 \text{ K}$. Sheffer et al. (2008), again using the same technique, find the average value of the excitation temperature of $J = 1$ relative to $J = 0$, $\langle T_{01}(\text{H}_2) \rangle = 77 \pm 17 \text{ K}$ for 56 lines of sight. This should be a good measure of the kinetic temperature. The range of T^k determined by HI absorption and emission studies (Heiles & Troland 2003) of the Cold Neutral Medium extends to somewhat lower temperatures, but the column density-weighted peak kinetic temperature is 70 K. The range $50 \text{ K} \leq T^k \leq 100 \text{ K}$ thus largely covers the measured range of kinetic temperatures determined for the

diffuse molecular clouds considered here.

6.3. Sources with J = 1–0 Observations Only

Of the 76 sources, 44 are in this category. The results are given in Table 4, for which we adopt $T^k = 100$ K. For the sources for which T_{10}^{ex} together with the statistical uncertainties define a range of allowed densities, we give the minimum and maximum H_2 densities, n_{min} and n_{max} . Given the statistical uncertainty in the excitation temperature, and the T_{10}^{ex} vs $n(H_2)$ curve seen in the lower panel of Figure 3, we consider that we have only an upper limit on the density of a source having $T_{10}^{ex} \leq 3.5$ K. We denote this maximum density n_{max} , and there is no entry for the minimum density n_{min} .

As is immediately seen in Figure 3, the dependence of the excitation temperature on the kinetic temperature for $n(H_2) \leq 100 \text{ cm}^{-3}$ is much smaller for the $J = 1-0$ transition than for the higher transitions. For most of the density range of interest, the change in $\log(n(H_2))$ required to achieve a particular T^{ex} is no more than 0.1 dex for kinetic temperature changing from 100 K to 50 K, and less than that for the kinetic temperature changing from 100 K to 150 K. The H_2 density required to achieve a given excitation temperature increases as the kinetic temperature decreases due to the reduced excitation rates; the $J = 3$ level is 33 K above the ground state. We adopt a kinetic temperature of 100 K for analysis of the $J = 1 - 0$ only clouds. The modest sensitivity to kinetic temperature indicates that our lack of knowledge of the kinetic temperature in a given cloud or the likely variation in the kinetic temperature throughout a single cloud will not produce a significant error in the derived value of the H_2 density compared to that resulting from the uncertainty in the excitation temperature arising from the imprecisely known column densities.

Of the 44 sources with only T_{10}^{ex} data, 30 have only upper limits on $n(H_2)$ and 14

have both lower and upper limits. The values of n_{max} for the former are relatively modest, all below 200 cm^{-3} , with the average value of $\log(n_{max})$ equal to 1.57, corresponding to $\langle n_{max} \rangle \simeq 37 \text{ cm}^{-3}$. This category includes, but is not restricted to, clouds having the lowest H_2 column densities. For each source the logarithm of the midpoint density, $\log(n_{mid})$ is the average of the logarithms of n_{max} and n_{min} . For the 14 sources with upper and lower limits, the average value of n_{min} is 22 cm^{-3} , and of n_{max} is 105 cm^{-3} . The average of the midpoint values of $\log(n(H_2))$ is 1.69 corresponding to $\langle n_{mid} \rangle = 49 \text{ cm}^{-3}$. These sources thus represent a population of diffuse clouds having relatively low densities. Thermal balance calculations indicate that these low density diffuse clouds will have relative high kinetic temperatures, thus justifying our adoption of 100 K for the nominal value of T^k .

6.4. Sources with Observations of Two or Three Transitions

Our sample includes 18 sources with two, and 14 sources with data for three transitions. The results for these 32 sources are given in Table 5. For each source we give the minimum and maximum density for each transition as discussed above, for kinetic temperature equal to 100 K. A dash indicates that there was no excitation temperature for that transition. In the last two columns we give the range of densities that satisfies all of the data available, if such a consistent range exists. Sources for which there is an upper limit only for a given transition have no entry in the appropriate n_{min} column.

For sources with data for more than one transition, there is the possibility of no density simultaneously yielding the different excitation temperatures even when the errors are included. For 18 sources, we find a range of densities consistent with all transitions observed. For 7 sources for which there was no formal consistent solution, an additional 0.1 dex in density allows a consistent density or density range to be found. These combined densities are indicated by an (s) by the derived density or density range. The absence of an

entry in both of the final two columns indicates there was no density consistent with the excitation temperatures for that source; there are 7 sources in this category.

We have 18 sources with data on T_{10}^{ex} and T_{21}^{ex} . Of these, 11 have a density range or upper limit consistent with the measurements of both transitions, while 3 additional sources are in this category if the additional 0.1 dex uncertainty is allowed. For the 12 sources with consistent density ranges, we find $\langle n_{min} \rangle = 22 \text{ cm}^{-3}$, and $\langle n_{max} \rangle = 70 \text{ cm}^{-3}$. The average value of the midpoint densities is $\langle \log(n_{mid}) \rangle = 1.63$ corresponding to $\langle n_{mid} \rangle = 43 \text{ cm}^{-3}$. This is slightly lower than, but certainly consistent with, the value obtained for the sources for which we have T_{10}^{ex} data only. This suggests that the two lowest CO transitions are not probing very different regions within or among diffuse molecular clouds along the line of sight.

We have 14 sources with data on excitation temperatures for 3 transitions. Since the three different excitation temperatures are differently sensitive to density, these sources are the most demanding in terms of defining a single characteristic density responsible for the entirety of the emission. Of these 14 sources, 7 have H_2 density ranges consistent with all three transitions, with 4 additional sources included if we allow the additional 0.1 dex in density added to range for each transition. For the 11 sources with consistent density range, we find $\langle n_{min} \rangle = 75 \text{ cm}^{-3}$, $\langle n_{max} \rangle = 118 \text{ cm}^{-3}$, and $\langle n_{mid} \rangle = 94 \text{ cm}^{-3}$. These values are somewhat higher than for the two previous categories, which suggests that inclusion of the $J = 3 - 2$ transition does tend to select out clouds or regions within clouds having somewhat higher densities. Given the uncertainties, the values of $\langle n_{mid} \rangle$ of 49, 42, and 94 cm^{-3} can be taken together to define an average density $\langle n_{mid} \rangle = 60 \text{ cm}^{-3}$ for the 36 sources with H_2 density ranges, again assuming a kinetic temperature $T^k = 100 \text{ K}$.

Of the 32 sources with multiple transition data, we obtain a consistent density ranges for 9 (50%) of those with the two lowest transitions, and 7 (50%) of those with three

transitions. If we include the stretch sources, these numbers go up to 12 (67%) and 10 (71%). Thus, the inclusion of sources with 3 as compared to 2 transitions leaves the fraction of sources for which a consistent density range can be found essentially unchanged. Of the 7 sources with no consistent density solution, 5 can be characterized as having the $J = 1-0$ transition implying too-low density (compared to $J = 2-1$ (4 sources) or to both $J = 2-1$ and $3-2$ (1 source)). The 2 remaining sources are characterized by having $J = 2-1$ transition implying a density range higher than that indicated by the $J = 1-0$ and $3-2$ transitions.

While the $J = 3-2$ transition data are suggestive of higher densities, it is not obvious that a density gradient or multiple density components affect level populations in a way that prevents obtaining a single density solution. In fact, the simple combination of two densities generally produces a solution that is simply an intermediate value. This is illustrated in Figure 5, in which we have combined two different clouds having densities of 10 cm^{-3} and 100 cm^{-3} with the low density component (cloud 1) having a fraction between 0 and 1 of the total CO column density. We assume that both clouds have the same kinetic temperature. Since all lines are optically thin, it is straightforward to calculate the excitation temperatures that would be derived from the relative column densities. The result is that the variation in the three excitation temperatures produced by varying the relative amount of high and low density cloud material mimics quite closely the variation in the excitation temperatures produced by a single cloud having density between that of the lower density and the higher density cloud.

6.5. Average Density and Thermal Pressure

The values for the H_2 density of each source have been found in terms of maximum and minimum values of $\log(n(\text{H}_2))$ that are consistent with the data including errors predominantly due to statistical uncertainties. The sources having 2 or 3 values of kinetic

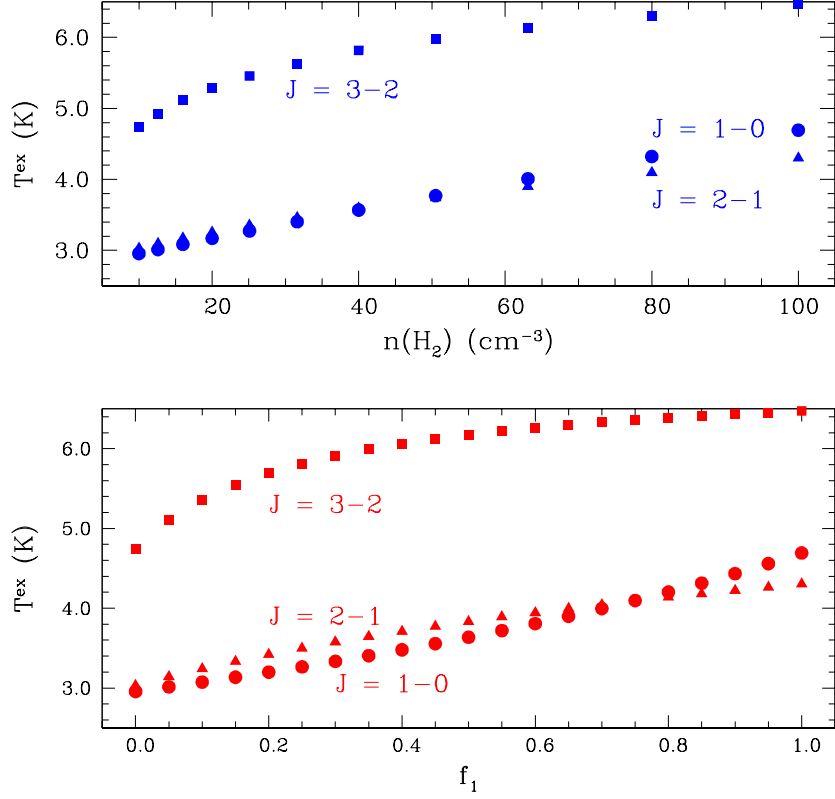


Fig. 5.— Comparison between varying the density within a single region and combining two regions having different densities. The kinetic temperature in all cases is 100 K and the background temperature is 2.7 K. Upper panel: excitation temperatures for three lowest CO transitions as function of H_2 density in a single region producing optically thin emission with $10 \text{ cm}^{-3} \leq n(\text{H}_2) \leq 100 \text{ cm}^{-3}$. Lower panel: excitation temperatures resulting from combination of two regions. Region 1 has $n(\text{H}_2) = 10 \text{ cm}^{-3}$ and region 2 has $n(\text{H}_2) = 100 \text{ cm}^{-3}$. The fraction of the total column density in region 1 is denoted f_1 . The three excitation temperatures show almost exactly the same variation in both cases, suggesting that a combination of 2 clouds with high and low densities is not distinguishable from a single cloud having an intermediate density.

temperature are likely to be the most valuable for assessing the effect of kinetic temperature changes since the different transitions have upper levels significantly higher than for the $J = 1-0$ transition, although there are relatively fewer of the multiple-transition sources. Figure 3 shows that while T_{10}^{ex} is relatively insensitive to T^k , the higher transitions show increasing sensitivity, as expected for the larger level separation (equivalent to 33 K for the $J=3-2$ transition). The collision rates increase monotonically with kinetic temperature in the range of interest, and thus the density required to obtain a given kinetic temperature is lower for a higher value of T^k .

In Figure 7 we show graphically the range of densities for each of the excitation temperatures in six sources in this category. As anticipated, the allowed densities are shifted to higher values for the lower kinetic temperature. This applies to the individual transitions as well as for the allowed ranges for the combined set of three transitions. For four of the six sources, the allowed density range for the combined set of transitions is substantial. However, for HD148937, the combined transition density range is very narrow, only 0.1 dex. For HD147683 there is nominally no density consistent with all three excitation temperatures, but $\log(n(\text{H}_2))$ is within 0.1 dex of the upper limit from the $J = 1-0$ transition and an equal amount from the lower limit of the $J = 2-1$ transition for $T^k = 100$ K, and similarly $\log(n(\text{H}_2)) = 2.5$ for $T^k = 50$ K. There is no obvious pattern from changing the kinetic temperature other than the shift to slightly higher densities for 50 K compared to 100 K kinetic temperature. It therefore does not seem possible to use the available data to put tighter constraints on the kinetic temperature; measurements of higher- J transitions would be required to do this.

We can find the average value of the midpoint density for several different groupings of our sources, and the results are given in Table 6. We see that $\langle n_{mid} \rangle$ is essentially the same for the 14 sources for which we have only T_{10}^{ex} and the 12 sources for which we have

values for T_{10}^{ex} and T_{21}^{ex} . For both categories, $\langle n_{mid} \rangle \simeq 45 \text{ cm}^{-3}$, at a kinetic temperature of 100 K. The minimum, maximum, and midpoint densities are all greater when we consider 3 rather than 2 excitation temperatures, as discussed above. If we include the 23 sources with 2 or 3 excitation temperatures the average value of the midpoint density is $\langle n_{mid} \rangle = 68 \text{ cm}^{-3}$, compared to 42 cm^{-3} for two excitation temperatures, and 94 cm^{-3} for three excitation temperatures, all for $T^k = 100 \text{ K}$.

For a lower kinetic temperature of 50 K, we obtain somewhat higher densities. For the sources with data on two excitation temperatures, $\langle n_{min} \rangle = 32 \text{ cm}^{-3}$, $\langle n_{mid} \rangle = 67 \text{ cm}^{-3}$, and $\langle n_{max} \rangle = 143 \text{ cm}^{-3}$. For the sources with data on three excitation temperatures, $\langle n_{min} \rangle = 104 \text{ cm}^{-3}$, $\langle n_{mid} \rangle = 135 \text{ cm}^{-3}$, and $\langle n_{max} \rangle = 176 \text{ cm}^{-3}$. All of these results are in line with previous determinations of densities of diffuse clouds. There do seem to be clear variations among the sources included in this study, with some sources having $n(\text{H}_2)$ only a few tens cm^{-3} (HD23478 and HD24398), while HD147888 has a density at least a factor of 10 higher.

The thermal pressure suggested by these results is moderately large. The anticorrelation between assumed T^k and derived $n(\text{H}_2)$ suggests that a thermal pressure derived by taking their product is reasonably robust against errors in the kinetic temperature. Using the midpoint densities for the sources with two or three values of excitation temperature as the largest statistical sample with reasonable sensitivity to kinetic temperature, we find for $T^k = 100 \text{ K}$, $p/k = 6800 \text{ Kcm}^{-3}$, and for $T^k = 50 \text{ K}$, $p/k = 4600 \text{ Kcm}^{-3}$. Further taking the average of these two yields a thermal pressure $p/k = 6700 \text{ Kcm}^{-3}$. This value is noticeably above the median value determined from UV absorption studies of CI by Jenkins & Tripp (2001), 2240 Kcm^{-3} , but within the range of the sources studied similarly by Jenkins (2002), $10^3 \text{ Kcm}^{-3} \leq p/k \leq 10^4 \text{ Kcm}^{-3}$. A more comprehensive CI study of 89 stars by Jenkins & Tripp (2011) finds a lognormal pressure distribution with $\langle \log(p/k) \rangle = 3.58$,

corresponding to $\langle p/k \rangle = 3800 \text{ Kcm}^{-3}$. It is possible that while the densities found here from CO are still quite modest, the regions may be the envelopes of molecular clouds, which are characterized by significantly higher thermal pressure than for diffuse molecular clouds (Wolfire, Hollenbach, & McKee 2010).

6.6. Correlation Between Volume Density and Column Density

The present data allow us to examine whether there is a correlation between volume density and column density for this sample of diffuse clouds. We have 14 sources with density ranges from T_{10}^{ex} alone and molecular hydrogen column densities. These are plotted with diamond (black) symbols in Figure 6. We also have 16 sources from our sample with density ranges determined by excitation temperatures from 2 (9 sources) and 3 (7 sources) transitions; these are plotted with square (red) symbols.

For the T_{10}^{ex} only sources, there is no significant correlation of volume and column density. The data for the multiple-transition sources suggests a weak correlation, with a linear best fit $n(\text{H}_2)$ rising from 10 cm^{-3} to 100 cm^{-3} as $N(\text{H}_2)$ increases from 10^{20} cm^{-2} to 10^{21} cm^{-2} . It is clear, however, that a linear relationship is not consistent with the data for HD 147888, which has a density $\simeq 4$ higher than the general trend. These data suggest that there is at least a component of diffuse molecular clouds for which volume density and column density are correlated.

7. Discussion and Summary

We have used the UV CO absorption data of Sheffer et al. (2008) and published data on other sources, together with statistical equilibrium calculations, to determine the volume density in diffuse interstellar molecular clouds. We have a total of 76 sources, of which 44

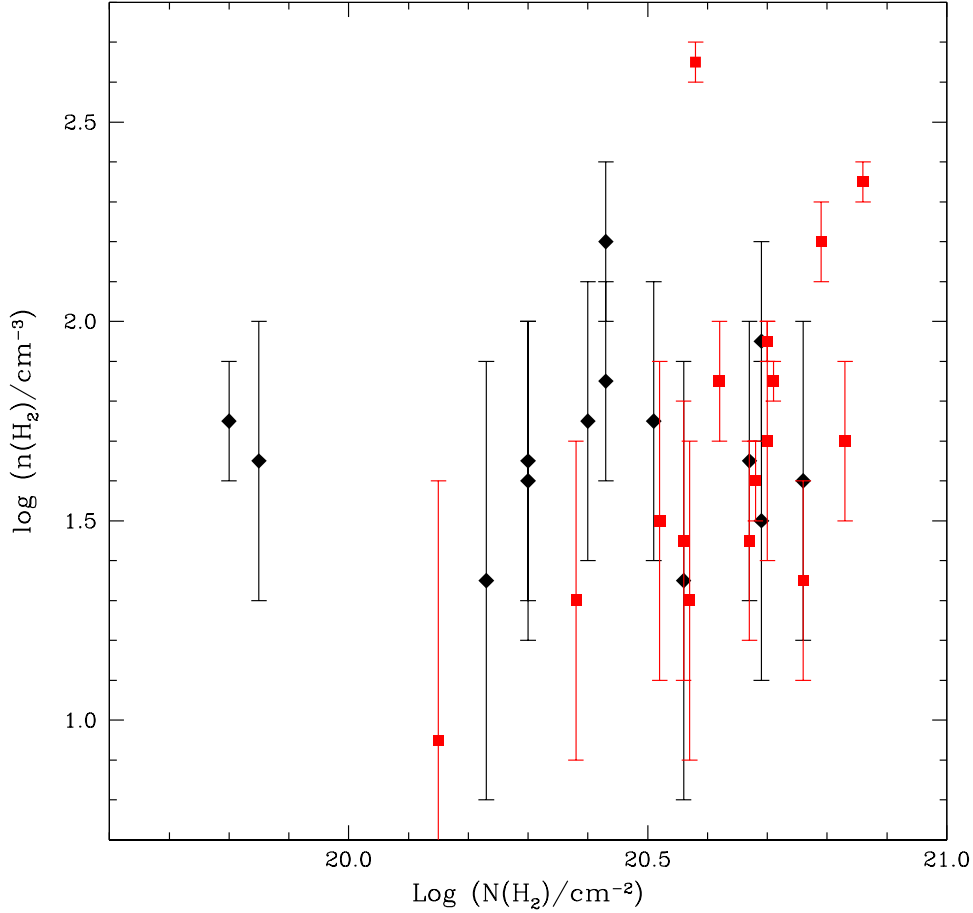


Fig. 6.— Volume density of H_2 determined from CO absorption as a function of H_2 column density. The sources included here have upper and lower density limits. Those from the $J = 1-0$ transition alone are plotted with diamond (black) symbols and those from sources with 2 or 3 excitation temperatures are plotted with square (red) symbols. The midpoint density for each source is indicated by the symbol and the upper and lower limits of the density range (Table 5) by the error bars. The source with the unusually high volume density is HD 147888. The sources with multiple transition data clearly show $n(\text{H}_2)$ correlated with $N(\text{H}_2)$, while those with $J = 1-0$ only data do not.

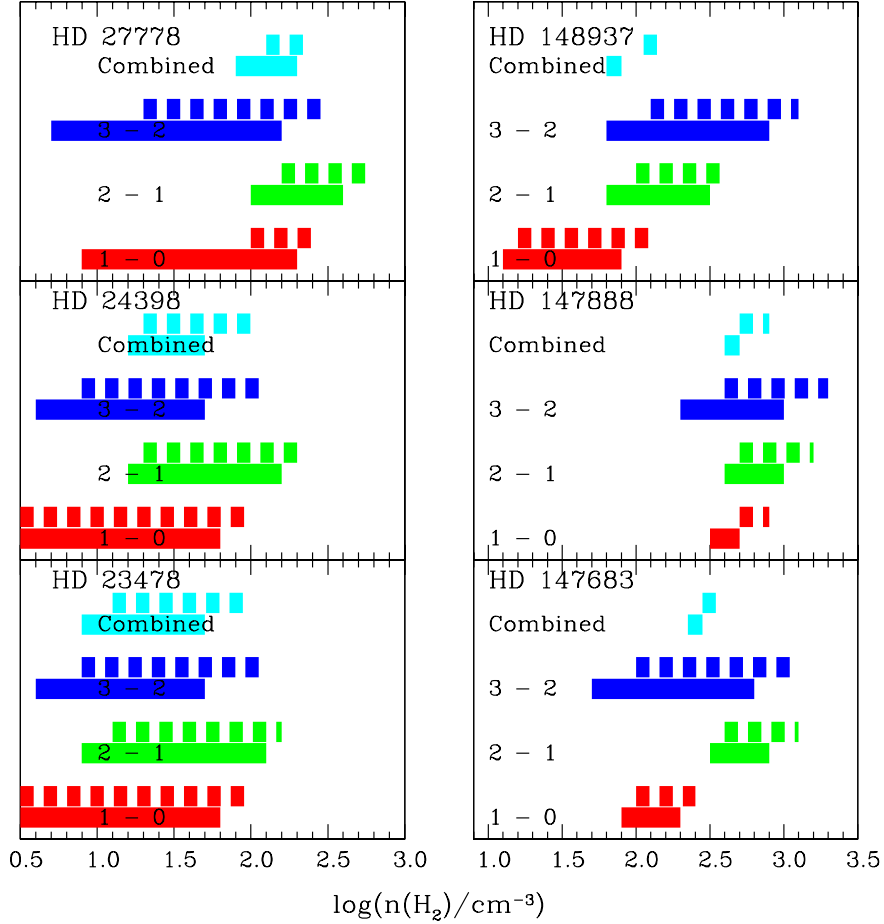


Fig. 7.— Volume density of H_2 determined from CO absorption towards six of the sources for which 3 excitation temperatures are determined. For each source, the ranges permitted (given assumed $\pm 20\%$ uncertainties) for each transition are indicated by the bars (red, green, and blue) in order of increasing transition frequency. The ranges for $T^k = 100$ K are indicated by the solid bars, and those for 50 K by the dashed bars plotted just above.

have T_{10}^{ex} data only, 18 sources having T_{10}^{ex} and T_{21}^{ex} data, and 14 sources having T_{10}^{ex} , T_{21}^{ex} , and T_{32}^{ex} data. It does not appear likely that non-collisional processes play a major role in excitation of CO in diffuse clouds. Collisional excitation is expected to result primarily from collisions with H_2 molecules as the H^0 to H_2 transition occurs at substantially lower values of column density than does the C^+-C^o-CO transition. Recent calculations confirm that excitation rate coefficients for CO- H_2 collisions are significantly larger than for CO- H^0 collisions. The CO and H_2 column densities of the sources indicate that the fractional abundance of CO is several orders of magnitude below its asymptotic value in well-shielded regions, and also that the CO rotational transitions are optically thin, with the sources having the largest CO column densities reaching $\tau \simeq 1$. We have assumed a kinetic temperature of 100 K as representative for the more diffuse clouds, but also discuss the effect of T^k a factor of 2 lower, especially for analysis of sources having data on higher $-J$ transitions.

For 30 of the sources having only T_{10}^{ex} data, we obtain only upper limit to $n(H_2)$ for which the average value is $\langle \log(n_{max}) \rangle = 1.57$, corresponding to $\langle n_{max} \rangle = 37 \text{ cm}^{-3}$. For the remaining 14 T_{10}^{ex} -only sources we find a range of H_2 densities that is consistent with the value of the excitation temperature and its estimated uncertainty, and thus determine n_{min} as well as n_{max} . For these sources we find $\langle n_{min} \rangle = 22 \text{ cm}^{-3}$ and $\langle n_{max} \rangle = 105 \text{ cm}^{-3}$. Defining $\log(n_{mid})$ as the average of $\log(n_{max})$ and $\log(n_{min})$ for each source, the average midpoint density for these 14 sources is given by $\langle n_{mid} \rangle = 49 \text{ cm}^{-3}$. Of the 18 sources having T_{21}^{ex} and T_{10}^{ex} data, 14 yield a consistent density range or upper limit. For the 12 sources with density ranges, $\langle n_{mid} \rangle = 42 \text{ cm}^{-3}$ for $T^k = 100 \text{ K}$ and 67 cm^{-3} for $T^k = 50 \text{ K}$. Of the 14 sources having T_{10}^{ex} , T_{21}^{ex} , and T_{32}^{ex} data, 11 yield density ranges that are consistent for all three transitions, yielding $\langle n_{mid} \rangle = 94 \text{ cm}^{-3}$ for $T^k = 100 \text{ K}$ and 135 cm^{-3} for $T^k = 50 \text{ K}$. Taking the sources with either two or three values of the excitation temperature, we find $\langle n_{mid} \rangle = 68 \text{ cm}^{-3}$ for $T^k = 100 \text{ K}$ and 92 cm^{-3} for $T^k = 50 \text{ K}$.

Thus, while there are undoubtedly some selection biases, it appears that this sample of diffuse molecular clouds, having H_2 column densities between $\text{few} \times 10^{20}$ and $\simeq 10^{21} \text{ cm}^{-2}$ is reasonably characterized by a density between 50 and 100 cm^{-3} . The clouds in this sample clearly do not all have the same volume density, with the extreme cases being a factor of a few below and above the range given here. The anticorrelation between derived density and the assumed kinetic temperature allows plausible determination of the internal thermal pressure of these clouds, which is found to be relatively large with p/k in the range 4600 to $6800 \text{ cm}^{-3}\text{K}$. As we are analyzing clouds in which hydrogen is largely molecular, but in which the fractional abundance of CO is so small that this species would be extremely difficult to detect in emission, the present results help characterize the “CO–Dark Molecular Component” of the interstellar medium.

We thank Drs. N. Balakrishnan and L. Wiesenfeld for very helpful information about collision rate coefficients and potential energy surfaces. We thank Nicolas Flagey and Jorge Pineda for useful discussions about dealing with the uncertainties in the column densities of CO and the rotational excitation temperatures, and Bill Langer for clarifying a number of points and a careful reading of the manuscript. The anonymous referee also made significant contributions by pointing out particular aspects of UV studies of diffuse clouds that would otherwise have been missed, and by carefully checking of the data presented here. This research was carried out at the Jet Propulsion Laboratory, California Institute of Technology, under contract with the National Aeronautics and Space Administration.

8. Appendix

8.1. INTRODUCTION

This appendix addresses the issue that the excitation temperature of the levels of simple molecules and atoms in the limit of very low densities does not asymptotically approach the temperature of the background radiation field. This applies to rigid rotor molecules such as CO, and also to simple atomic systems such as CI and OI.

Using the RADEX program (Van der Tak et al. 2007) to analyze CO excitation by collisions with ortho-H₂ molecules for a kinetic temperature of 100 K, background temperature of 2.7 K, and H₂ density of 0.01 cm⁻³ yields the results shown in Table 7. All transitions are optically thin, and since collisional deexcitation rate coefficients are \simeq few $\times 10^{-11}$ cm³s⁻¹, all transitions should be highly subthermal, given that the *A*-coefficient for the lowest transition is 7.2×10^{-8} s⁻¹.

This result, that the excitation temperatures seem unreasonably large and increase with increasing *J* (albeit not perfectly monotonically), is found in the output of all statistical equilibrium programs examined. It thus does not seem to be an artifact of the calculation, but rather is a property of the solutions of the rate equations in the low density limit. While this may seem to be a curiosity, it is important if one has level populations derived from UV absorption, for example, and one wishes to solve for densities that result in highly subthermal excitation. This is suggested by the FUSE and HST observations of CO of Sheffer et al. (2008) and others that are discussed in this paper.

8.2. Three Level Model

8.2.1. Definitions

In order to gain some insight into the behavior of the excitation temperatures, we can use a three level model with two transitions to capture the essence of the multilevel CO problem. This is a complete representation of the situation for atomic CI and OI fine structure systems and a very good approximation for CO at low densities. We denote the levels 1, 2, and 3 (not to be confused with rotational quantum numbers), their energies as E_1 , E_2 , and E_3 , and the downwards spontaneous rates and collision rates as A_{21} , A_{32} , C_{21} , C_{32} , and C_{31} . The energies of the three levels lead to equivalent temperatures for the three transitions $kT_{21} = E_2 - E_1$, $kT_{32} = E_3 - E_2$, and $kT_{31} = E_3 - E_1$, where k is Boltzmann's constant. The background radiation field is assumed to be a blackbody at temperature T^{bg} producing energy density $U(T^{bg})$. The downwards stimulated rates are $B_{21}U$ and $B_{32}U$, where the B 's are the stimulated radiative rate coefficients and U is understood to be evaluated at the frequency of the transition in question. The upwards stimulated rates are related to the downwards rates through the statistical weights g_1 , g_2 , and g_3 and detailed balance, giving $g_1B_{12}U = g_2B_{21}U$ and $g_2B_{23}U = g_3B_{32}U$.

The collision rates are the product of the collision rate coefficients and the colliding partner density. Thus for collisions with H_2 ,

$$C_{ij} = R_{ij}n(H_2) \quad (10)$$

The upwards rates are related to the downwards rates through detailed balance and the kinetic temperature T_k through $g_1C_{12} = g_2C_{21}\exp(-T_{21}^*/T^k)$, $g_1C_{13} = g_3C_{31}\exp(-T_{31}^*/T^k)$, and $g_2C_{23} = g_3C_{32}\exp(-T_{32}^*/T^k)$.

The level population per statistical weight defines the excitation temperature through equation 1. With these definitions, the rate equations for the level populations n_1 , n_2 , and

n_3 lead to the following equations for the ratios of the column densities of adjacent levels (connected by radiative transitions):

$$\frac{N_2}{N_1} = \frac{(A_{32} + B_{32}U + C_{32} + C_{31})(B_{12}U + C_{12} + C_{13}) - C_{13}C_{31}}{(A_{32} + B_{32}U + C_{32} + C_{31})(A_{21} + B_{21}U + C_{21}) + (C_{23} + B_{23}U)C_{31}} , \quad (11)$$

and

$$\frac{N_3}{N_2} = \frac{(C_{23} + B_{23}U)(B_{12}U + C_{12} + C_{13}) + (A_{21} + B_{21}U + C_{21})C_{13}}{(A_{32} + B_{32}U + C_{32} + C_{31})(B_{12}U + C_{12} + C_{13}) - C_{13}C_{31}} . \quad (12)$$

8.2.2. High Density Limit

In this limit with $C \gg A, BU$, we find that equations 11 and 12 yield $N_2/N_1 = (g_2/g_1)e^{(-T_{21}^*/T^k)}$ and $N_3/N_2 = (g_3/g_2)e^{(-T_{32}^*/T^k)}$, respectively. This is exactly as expected in the thermalized limit when collisions dominate.

8.2.3. Zero Collision Rate Limit

In this limit

$$\frac{N_2}{N_1} = \frac{B_{12}U}{A_{21} + B_{21}U} , \quad (13)$$

and

$$\frac{N_3}{N_2} = \frac{B_{23}U}{A_{32} + B_{32}U} . \quad (14)$$

which yield $T^{ex} = T^{bg}$ for both transitions.

8.2.4. Low Density Limit with No Background Radiation

With the above expressions we can examine the low density limit, together with the effect of varying the background radiation temperature. We first consider the no-background

limit ($T^{bg} = 0$). In this case, dropping collisional terms where they compete directly with a spontaneous rate, we find

$$\frac{N_2}{N_1} = \frac{C_{12} + C_{13}}{A_{21}} , \quad (15)$$

and

$$\frac{N_3}{N_2} = \frac{A_{21}C_{13} + C_{23}(C_{12} + C_{13})}{A_{32}(C_{12} + C_{13})} . \quad (16)$$

If the $\Delta J = 2$ collision rate coefficients are zero, equation 16 reduces to

$$\frac{N_3}{N_2} = \frac{C_{23}}{A_{32}} . \quad (17)$$

In this case of purely “dipole-like” collisions, we also find

$$\frac{N_2}{N_1} = \frac{C_{12}}{A_{21}} , \quad (18)$$

We thus see that the excitation temperature of each transition approaches zero as the collision rate approaches zero.

If collisions between levels 1 and 3 are allowed, then in the limit of very low collision rate, we find

$$\frac{N_3}{N_2} = \frac{A_{21}}{A_{32}} \frac{C_{13}}{C_{12} + C_{13}} . \quad (19)$$

This obviously has an entirely different behavior than that of the lower transition given by equation 15. The excitation temperature of the upper transition approaches an asymptotic limit since the first fraction is a constant determined by the molecular radiative rates, and the second fraction is a constant determined by the relative collision rates. For the latter, in the limit of zero background, the excitation temperature for the upper transition is **independent of the density**, and is given by

$$T_{32}^{ex} = T_{32}^* / \ln \left[\frac{g_3 A_{32}}{g_2 A_{21}} \left(\frac{R_{12} + R_{13}}{R_{13}} \right) \right] . \quad (20)$$

In the low density limit (with no background), the excitation temperature for the lower transition is

$$T_{21}^{ex} = T_{21}^* / \ln \left[\frac{g_2}{g_1} \frac{A_{21}}{C_{12} + C_{13}} \right] , \quad (21)$$

which **does** depend on the collision partner density through the proportionality of the collision rates and the density (equation 10).

To restate the obvious, the excitation temperature of the upper (level 3 – level 2) transition does not approach zero even if the collision rate is arbitrarily small. This is because there is not a simple competition between collisional and radiative processes. This is in contrast with the lower (level 2 – level 1) transition, for which the excitation temperature does approach zero for low collision rate. This reflects the fact that in the limit of very infrequent collisions, level 2 is populated exclusively by collisions from level 1 (which has most of the population) and depopulated by radiative decay back to level 1.

It is thus evident that the excitation temperature of a particular transition in a multilevel system can behave in the apparently counterintuitive way of having T^{ex} not approach zero as the collision rate approaches this value. We next give some examples of three-level systems, and will extend the discussion to systems with more than 3 levels in Section 8.3

8.2.5. *Examples of Different Systems and Comparisons with Numerical Calculations*

8.2.6. *CO*

We consider the lowest three rotational levels of CO to illustrate the preceding analytic results. The rate coefficients for collisions with para-H₂ from Yang et al. (2010) at a kinetic temperature of 100 K are $R_{12} = 9.7 \times 10^{-11} \text{ cm}^3\text{s}^{-1}$ and $R_{13} = 1.4 \times 10^{-10} \text{ cm}^3\text{s}^{-1}$. Since the collision rates and rate coefficients are proportional (equation 10), this gives $(R_{12} + R_{13})/R_{13} = 1.7$, which yields (for no background radiation) $T_{32}^{ex} = 3.35 \text{ K}$. The collisional excitation rates for ortho-H₂ – CO collisions from Flower (2001) and Wernli et al. (2006) as extrapolated in the LAMDA database (home.strw.leidenuniv.nl/moldata/)

at a kinetic temperature of 100 K are $R_{12} = 2.65 \times 10^{-10} \text{ cm}^3\text{s}^{-1}$ and $R_{13} = 2.63 \times 10^{-10} \text{ cm}^3\text{s}^{-1}$. This gives $(R_{12} + R_{13})/R_{13} = 2.1$ and an excitation temperature (for no background radiation) $T_{32}^{ex} = 3.2 \text{ K}$. The value from the full multilevel RADEX calculation is 3.6 K. The difference is due to the effect of the higher levels, discussed in Section 8.3.

T_{32}^{ex} is essentially constant for H_2 densities up to 100 cm^{-3} , at which point it begins to rise due to the collision rate becoming comparable to the spontaneous decay rate. The excitation temperature of the lower transition, as expected, varies continuously as a function of the H_2 density. This behavior is shown in Figure 8. The excitation temperature of the lower transition is rising sharply as $n(\text{H}_2)$ approaches 100 cm^{-3} , because with the relatively large rate for $\Delta J = 2$ collisions, we can have a situation in which level 3 ($J = 2$) is populated by collisions from level 1 ($J = 0$). The radiative decays to level 2 ($J = 1$) add to the direct collisional population of that level and result in level 2 ($J = 1$) becoming overpopulated relative to level 1 ($J = 0$) as seen in Goldsmith (1972). As the H_2 density increases, the negative excitation temperatures characteristic of the population inversion are preceded by very high positive values of the excitation temperature of the lowest transition, T_{21}^{ex} .

The behavior of T_{32}^{ex} is largely independent of the choice of collision partner or which calculation of the collision rate coefficients is adopted. The Green & Thaddeus (1976) rate coefficients for CO-H_2 collisions give $(R_{12} + R_{13})/R_{13} = 1.61$ and $T_{32}^{ex} = 3.4 \text{ K}$, almost identical to the results from Yang et al. (2010), although the values for the individual coefficients are slightly larger. Green & Thaddeus (1976) also give the results for collisions with H and He atoms, which give $T_{32}^{ex} = 3.3 \text{ K}$ and 3.47 K , respectively, almost identical to the values produced by collisions with H_2 molecules.

8.2.7. CI

The three fine structure levels of CI make this system a highly appropriate test of this behavior for low collision rates. The ground state (level 1) is 3P_0 , the first excited state (level 2 at $E/k = 23.65$ K above the ground state) is 3P_1 , and the second excited state (level 3 at 62.51 K above the ground state) is 3P_2 . Adopting the deexcitation rate coefficients of Schröder et al. (1991) for collisions with ortho- H_2 , we find for a kinetic temperature of 100 K that $R_{12} = 1.68 \times 10^{-10} \text{ cm}^3\text{s}^{-1}$ and $R_{13} = 1.85 \times 10^{-10} \text{ cm}^3\text{s}^{-1}$. With $A_{32} = 2.65 \times 10^{-7} \text{ s}^{-1}$ and $A_{21} = 7.9 \times 10^{-8} \text{ s}^{-1}$, we find from equation 20 that $T_{32}^{ex} = 16.7$ K. The excitation temperature of the lower transition from equation 21 is 3.65 K for a hydrogen density of 1 cm^{-3} and no background radiation. The value for the upper transition agrees within a few tenths K with that from RADEX, and that of the lower transition agrees within 0.1 K.

8.2.8. Effect of Background Radiation

The ratio of the downwards stimulated emission rate due to the background radiation field to the spontaneous decay rate is given by

$$\frac{B_{ul}U}{A_{ul}} = \frac{1}{\exp(T^*/T^{bg}) - 1} , \quad (22)$$

where T^{bg} is temperature of the background radiation field, which we assume to be a blackbody. Let us consider the situation in which $C_{ul} \ll A_{ul}$ with no background radiation field ($T^{bg} = 0$). If we consider increasing the background temperature, we will reach a point at which $B_{ul}U = C_{ul}$. This occurs when

$$T^{bg'} = \frac{T^*}{\ln(1 + A_{ul}/C_{ul})} . \quad (23)$$

The required background temperature thus depends on how much smaller the collision rate is than the spontaneous rate. For this value of background temperature, we should expect

the excitation temperature to approach the background temperature since spontaneous and stimulated rates are both comparable to or greater than the collision rate. The results for the 3 level model for CO are shown in Figure 9, for a kinetic temperature of 100 K and a H₂ density of 1 cm⁻³. At this density, $A_{21}/C_{21} = 2.1 \times 10^3$ and $A_{32}/C_{32} = 1.1 \times 10^4$.

Equation 23 gives $T^{bg'} = 0.7$ K for the lower transition and 1.2 K for the higher transition, both of which are in reasonable agreement with Figure 9. Since T^{ex} for the lower transition is less than $T^{bg'}$, the excitation temperature increases as T^{bg} increases. As discussed previously, the excitation temperature of the higher transition is relatively large with no background present, and so it initially drops as T_{bg} increases, before joining the $T^{ex} = T^{bg}$ curve.

For this density and the two lower transitions, $T^{bg'}$ is significantly smaller than the background temperature required to make $B_{ul}U = A_{ul}$, which is just $T^{bg''} = T^*/\ln(2) = 1.44T^*$. We can see from the excitation temperatures given in Table 7 that the stimulated rate produced by a background temperature equal to 2.7 K is sufficient to bring the excitation temperatures of two lowest transitions close to equilibrium with the background temperature. For the higher transitions, the blackbody radiation function falls off sufficiently rapidly that the background becomes insignificant, and the rise of the excitation temperature as one moves up the ladder is essentially the same as from that with no background present at all.

8.3. Systems with More than Three Levels

Analytic solution of the level populations in systems having many levels is in general tedious. The exception is for dipole-like collisions for which only adjacent levels are coupled. In this situation the ratio of column densities of any pair of adjacent levels can be written

$$\frac{N_u}{N_l} = \frac{B_{lu}U + C_{lu}}{A_{ul} + B_{ul}U + C_{ul}}, \quad (24)$$

analogous to equation 17 and 18, but in which the background radiation can be included.

If collisions connect non-adjacent levels, one typically resorts to numerical solutions based on matrix inversion. In the low collision rate limit, the population (for no background radiation) will be limited to the lowest level, since the collisional excitation rate is by assumption less than any spontaneous decay rate. In the case of low but nonzero collision rate, the population will be restricted to the lowest few levels. This will also be the case if there is a background radiation field that produces a stimulated rate comparable to the collision rate for only the lowest few transitions. For a molecule with simple rotor structure, the analytic solution for no background radiation yields an equation similar to equation 19, but with some modifications due to the collisions that change the rotational quantum number by a range of integers.

We can write the population ratio of pair of levels u and l in the absence of any background radiation as

$$\frac{N_u}{N_l} = \frac{A_{l-1} \sum_{k=u}^{k=k_{max}} C_{1k}}{A_{ul} \sum_{k=l}^{k=k_{max}} C_{1k}} \quad (25)$$

where $l - 1$ indicates the level below the lower level of the pair in question, and k_{max} is the highest level that is connected by collisions to level 1 or the highest level included in the calculation. The limits on the summation in the numerator reflect the fact that collisions from the lowest level to levels above the upper level of the pair of interest all decay radiatively much faster than any collisional process, and thus effectively populate the upper level of the pair. The sum in the denominator yields the total rate of collisions that populate both members of the pair of levels of interest.

Equation 25 can be used to obtain the expression for the excitation temperature

$$T_{ul}^{ex} = T_{ul}^* / \ln \left[\frac{g_u}{g_l} \frac{A_{ul}}{A_{l-1}} P_{ul} \right] , \quad (26)$$

where the P_{ul} term reflects the collisional population rates and can be written

$$P_{ul} = 1 + C_{1l} / \sum_{k=u}^{k=k_{max}} C_{1k} . \quad (27)$$

The fractional population of the higher levels will be very small in this limit, but as seen from Table 7, the excitation temperatures are well-defined. It may seem surprising that the higher levels in this case are populated by collisions directly from the lowest level (or levels). We can verify this numerically, and for simplicity set the background radiation temperature to zero. We use the collision rate coefficients for ortho-H₂ CO collisions from Flower (2001) and Wernli et al. (2006) as extrapolated in the LAMDA database (home.strw.leidenuniv.nl/~moldata/), and for definitiveness consider CO rotational levels 20 and 19. The collisional deexcitation rate coefficients are $R_{20\ 1} = 7.5 \times 10^{-17} \text{ cm}^3 \text{ s}^{-1}$ and $R_{20\ 19} = 1.1 \times 10^{-10} \text{ cm}^3 \text{ s}^{-1}$. At a kinetic temperature of 100 K, the excitation rates are $R_{1\ 20} = 2.7 \times 10^{-20} \text{ cm}^3 \text{ s}^{-1}$ and $R_{19\ 20} = 3.9 \times 10^{-11} \text{ cm}^3 \text{ s}^{-1}$. The ratio of the rates of population of level 20 from level 1 to that from level 19 is given by

$$\frac{\text{population rate from level 1}}{\text{population rate from level 19}} = \frac{N_1 R_{1\ 20}}{N_{19} R_{19\ 20}} , \quad (28)$$

which in the present case is equal to 2×10^8 . It is thus clear that collisions that transfer population from the lowest level (or few lowest levels) to high-lying levels are the dominant excitation mechanism for the higher rotational levels of CO in the low density limit.

Returning to the issue of the expected excitation temperatures for high-J transitions, we must evaluate equation 26. There are two factors that must be considered to estimate the sum of the collisions to the levels above the upper level of the transition of interest. First, the collisional deexcitation rates decrease as ΔJ increases. Second, the upwards rates

(from the ground state) are further reduced by the increasing upper level energy, even for a moderately high kinetic temperature of 100 K. The result is that the rate to the lower level of the transition is significantly larger than that to the upper and to higher-lying levels.

If we consider the transition between levels 10 and 9 ($J = 9-8$) with ortho- H_2 collisions (as discussed above) at 100K, we find $P_{10\ 9} = 3.16$, which results in $T_{10\ 9}^{ex} = 30.7$ K. This agrees (fortuitously) well with the 30.6 K Radex result given in Table 7. For the transition between levels 18 and 17 ($J = 17 - 16$), $P_{18\ 17} = 5.5$, which results in $T_{18\ 17}^{ex} = 48.4$ K. This compares to the RADEX result $T_{18\ 17}^{ex} = 49.6$ K (Table 7). Given we included excitation only up to level 20, the agreement is very satisfactory.

8.4. Conclusions

We have analyzed the initially surprising behavior of the excitation of the CO rotational ladder under conditions of very low density, for which the excitation temperature increases steadily as one moves from lower to higher levels. The same effect is generally observed for rigid rotors, for simple atomic fine structure systems, as well as for molecules with more complex term schemes. This behavior can be understood by considering the limit in which collisional deexcitation can be ignored. Radiative decay then makes the population of all levels other than the ground state quite small. A (rare) collision from the ground state to an excited state is followed by a radiative cascade. The populations of the upper and lower levels of a transition are determined by the collisions into the respective levels, plus the radiative cascade from higher levels. The result is level populations that depend essentially only on the relative magnitudes of the A-coefficients for decay into and out of the lower level of the transition of interest. In consequence, the excitation temperature is proportional to the equivalent temperature $T^* = hf/k$ of the transition. The impact on the lower levels of CO is modest because the stimulated transition rate from the cosmic

microwave background radiation is sufficient to make the excitation temperature equal to the background temperature. The same is not true for the higher levels, for which the background is unimportant.

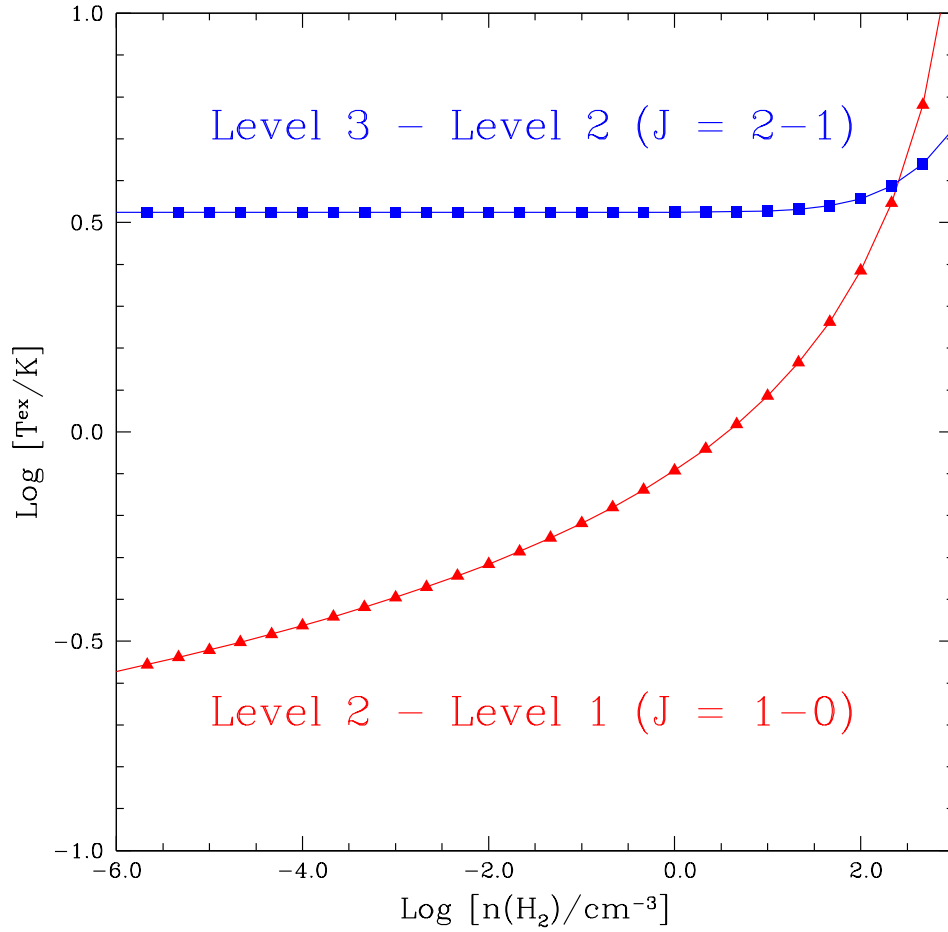


Fig. 8.— Excitation temperature of two lowest rotational transitions of CO as a function of H_2 density. There is no background radiation field, and the kinetic temperature is 100 K.

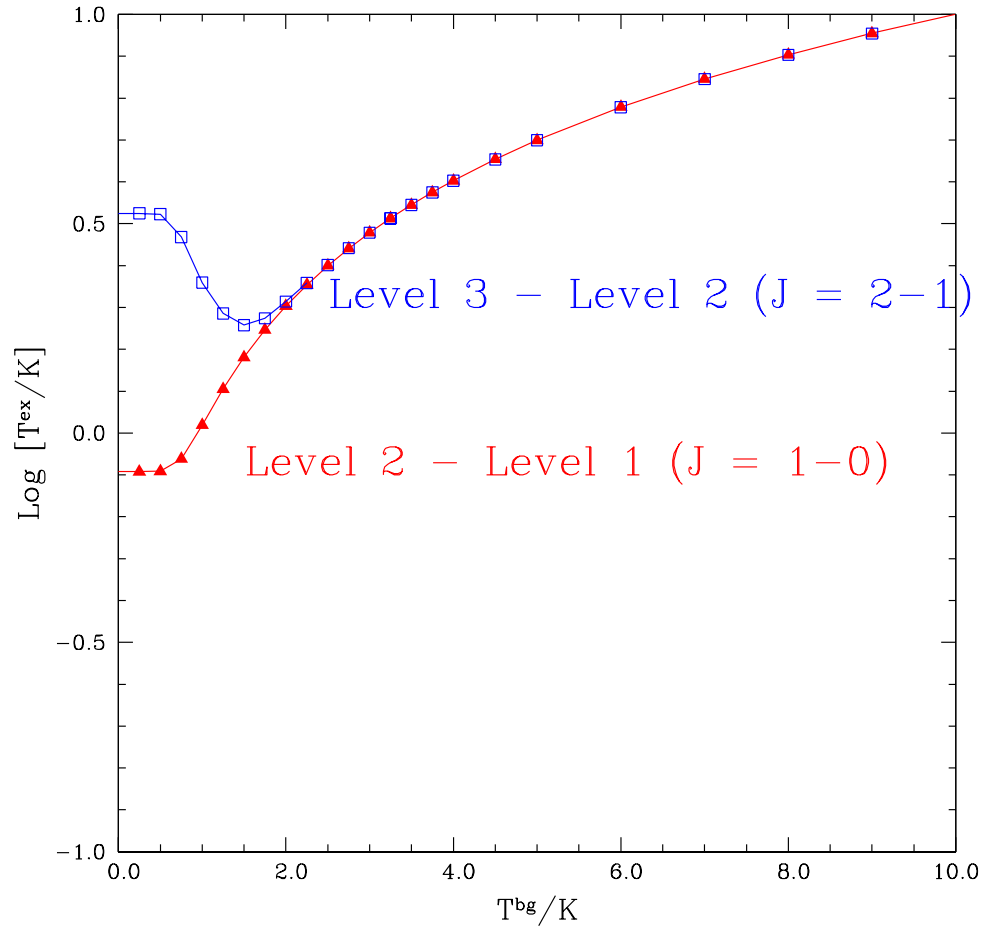


Fig. 9.— Excitation temperature for two lowest transitions of CO (labeled by rotational quantum number) as a function of the background radiation temperature T^{bg} . The kinetic temperature is 100 K and the H_2 density is 1 cm^{-3} .

REFERENCES

- Balakrishnan, N., Yan, M., & Dalgarno, A. 2002, *ApJ*, 568, 443
- Burgh, E.B., France, K., & McCandliss, S.R. 2007, *ApJ*, 658, 446
- Chandra, S., Maheshwari, V.U., & Sharma, A.K. 1996, *A&AS*, 117, 557
- Chu, S.-I. & Dalgarno, A. 1975, *Proc. R. Soc. Lond. A.*, 342, 191
- Cologne Database for Molecular Spectroscopy (CDMS) www.astro.uni-koeln.de/cdms/catalog
- Crawford, O.H. & Dalgarno, A. 1971, *J. Phys. B.*, 4, 494
- Dickinson, A.S. & Richards, D. 1975, *J. Phys. B*, 8, 2846
- Dickinson, A.S., Phillips, T.G., Goldsmith, P.F., et al. 1977, *A&A*, 54, 645
- Draine, B.T. 1978, *ApJS*, 36, 595
- Elitzur, M., and Watson, W.D. 1978, *ApJ*, 222, L141
- Federman, S.R., Glassgold, A.E., Jenkins, E.B., & Shaya, E.J. 1980, *ApJ*, 242, 545
- Federman, S.R., Rawlings, J.M.C., Taylor, S.D., & Williams, D.A. 1996, *MNRAS*, 279, L41
- Federman, S.R., Lambert, D.L., Sheffer, Y., et al. 2003, *ApJ*591, 986
- Green, S. & Thaddeus, P. 1976, *ApJ*, 205, 766
- Flower, D.R. 2001, *J. Phys. B.*, 34, 2731
- Godard, B., Falgarone, E., & Pineau des Forêts, G. 2009, *A&A*, 495, 847
- Goldsmith, P.F. 1972, *ApJ*, 176, 597

- Goldsmith, P.F., Langer, W.D., Pineda, J.L., & Velusamy, T. 2012, ApJS, 203, 13
- Heiles, C. & Troland, T.H. 2003, ApJ, 586, 1067
- Jenkins, E.B., Drake, J.F., Morton, D.C. 1973, ApJ, 181, L122
- Jenkins, E.B. & Tripp, T.M. 2001, ApJS, 137, 297
- Jenkins, E.B. 2002, ApJ, 580, 938
- Jenkins, E.B. & Tripp, T.M. 2011, ApJ, 734, 65
- Kavars, D.W., Dickey, J.M., McClure-Griffiths, N.M., et al. 2005, ApJ, 626, 887
- Lambert, D.L., Sheffer, Y., Gilliland, R.L., & Federman, S.R., 1994, ApJ, 420, 756
- Langer, W. D., Velusamy, T., Pineda, J. L., et al. 2010, A&A, 521, L17
- Le Petit, F., Nehemé, C., Le Bourlot, J., & Roueff, E. 2006, ApJS, 164, 506
- Liszt, H.S. & Lucas, R. 1998, A&A, 339, 561
- Liszt, H.S. 2006, A&A, 458, 507
- Pilbratt, G. L., Riedinger, J. R., Passvogel, T., et al. 2010, A&A, 518, L1
- Pineda, J.L., Langer, W.D., Velusamy, T., & Goldsmith, P.F. 2013, A&A, 554, A103
- Rachford, B.L., Snow, T.P., Tumlinson, J., et al. 2002, ApJ, 577, 221
- Savage, B.D., Bohlin, R.C., Drake, J.F., & Budich, W. 1977, ApJ, 216, 291
- Schröder, K., Staemmler, V., Smith, M.D., Flower, D.R., & Jaquet, R. 1991, J. Phys. B:
At. Mol. Opt. Phys., 24, 2487
- Sheffer, Y., Rogers, M., Federman, S.R., et al. 2007, ApJ, 667, 1002

- Sheffer, Y., Rogers, M., Federman, S.R. et al. 2008, *ApJ*, 687, 1075
- Shepler, B.C., Yang, B.H., Kumar, T.J.D., et al. 2007, *A&A*, 475, L15
- Snow, T.P. & McCall, B.J. 2006, *ARA&A*, 44, 367
- Sonnentrucker, P., Welty, D.E., Thorburn, J.A., & York, D.G. 2007, *ApJS*, 168, 58
- UMIST RATE2012 www.udfa.net
- Van Dishoeck, E.F. & Black, J.H. 1988, *ApJ*, 334, 771
- Van der Tak, F.F.S., Black, J.H., Schöier, F.L., Jansen, D.J., van Dishoeck, E.F. 2007, *A&A*468, 627
- Visser, R., van Dishoeck, E.F., & Black, J.H. 2009, *A&A*, 503, 323
- Wannier, P.G., Penpraes, B.E., & Andersson, B.-G. 1997, *ApJ*, 487, L65
- Welty, D.E. & Hobbs, L.M. 2001, *ApJS*, 133, 345
- Wernli, M., Valiron, P., Faure, A., et al. 2006, *A&A*, 446, 367
- Wolfire, M, Hollenbach, D., & McKee, C.F. 2010, *ApJ*, 716, 1191
- Yang, B., Stancil, P.C., Balakrishnan, N., & Forrey, R.C. 2010, *ApJ*, 718, 1062
- Yang, B., Stancil, P.C., Balakrishnan, N., et al. 2013, [arXiv1305.2376v1](https://arxiv.org/abs/1305.2376v1)
- Zsargó, J. & Federman, S.R. 2003, *ApJ*, 589, 319

Table 1. CO Excitation Temperatures¹ and H₂ Column Densities from Sheffer et al.
(2008) Unless Otherwise Indicated

Source	T ₁₀ ^{ex}	T ₂₁ ^{ex}	T ₃₂ ^{ex}	log (N(H ₂)/cm ⁻²)
BD +48 3437	2.7			20.42
BD +53 2820	3.3			20.15
CPD -69 1743	2.7			19.99
CPD -59 2603	3.0	3.5		20.15
HD 12323	3.1	5.3		20.32
HD 13268	3.4			20.51
HD 13745	4.0			20.67
HD 14434	4.4			20.43
HD 15137	3.1	5.1		20.32
HD 23478	3.4	3.7	5.0	20.57
HD 24190	3.1	3.7		20.38
HD 24398	3.4	4.0	5.0	20.67
HD 27778	5.3	5.6	5.7	20.79 ²
HD 30122	3.8	4.1		20.70
HD 36841	2.7	3.2		20.4 ³
HD 37367	3.2			20.61
HD 37903	2.7			20.95
HD 43818	4.1			20.4 ³
HD 58510	2.9			20.23
HD 63005	3.6			20.23
HD 91983	2.7			20.23
HD 93205	2.8			19.83
HD 93222	3.3			19.84
HD 93237	3.1			19.80
HD 93840	3.1			19.28

Table 1—Continued

Source	T_{10}^{ex}	T_{21}^{ex}	T_{32}^{ex}	$\log (N(\text{H}_2)/\text{cm}^{-2})$
HD 94454	3.8			20.76
HD 96675	3.7	8.4		20.86
HD 99872	3.7	3.9		20.52
HD 102065	3.6			20.56
HD 106943	2.7			19.81
HD 108002	3.2			20.34
HD 108639	3.0			20.04
HD 110434	2.7			19.90
HD 112999	3.0			20.11
HD 114886	3.1			20.34
HD 115071	3.7			20.69
HD 115455	2.9			20.58
HD 116852	3.2			19.83
HD 122879	2.9			20.36
HD 124314	3.4			20.52
HD 137595	3.9	4.7		20.62
HD 140037	2.9			19.34
HD 144965	4.3	6.0		20.79
HD 147683	5.2	7.4	7.4	20.74
HD 147888	13.6	8.0	8.7	20.58
HD 148937	3.7	4.9	7.7	20.71 ⁴
HD 152590	4.1			20.51
HD 152723	4.0			20.30
HD 154368	3.0	5.5		20.16 ²
HD 157857	4.6			20.69

Table 1—Continued

Source	T_{10}^{ex}	T_{21}^{ex}	T_{32}^{ex}	$\log (N(\text{H}_2)/\text{cm}^{-2})$
HD 163758	4.0			19.85
HD 177989	3.3	3.6		20.15 ⁴
HD 190918	2.7	5.3		19.95
HD 192035	3.2	4.4		20.68
HD 195965	3.0			20.34
HD 198781	3.4	3.9		20.56
HD 203532	5.3	4.6		20.70
HD 208905	6.0			20.43
HD 209481	2.9			20.54
HD 209975	2.9			20.15
HD 210809	3.1			20.00
HD 220057	3.0	4.4		20.34
HD 303308	3.1			20.15
HD 308813	3.8			20.30

¹Excitation temperatures derived from data given in Sheffer et al. (2008), using equations 2 – 4 in the present paper.

² $N(\text{H}_2)$ from Rachford et al. (2002).

³Estimates of $N(\text{H}_2)$ by Sheffer et al. (2008) based on correlations with column densities of other species.

⁴ $N(\text{H}_2)$ from Sheffer et al. (2007).

Table 2. Excitation Temperatures of CO Transitions and H₂ Column Densities from Other Sources

Source	T ₁₀ ^{ex} (K)	T ₂₁ ^{ex} (K)	T ₃₂ ^{ex} (K)	log (N(H ₂)/cm ⁻²)	Note
HD24534	4.6±1.7	5.6±0.4	5.6±1.0	20.92	a
HD104705	3.4±0.8			19.98	b
HD147933	2.7±0.1	7.6±0.5	8.4±0.5	20.53	c
HD148184	3.0±0.3	5.2±0.6	7.5±3.7	20.63	c
HD149757	3.4±0.4	4.5±0.2	5.9±0.5	20.62	d
HD185418	3.3±0.3	4.0±1.2		20.76	a
HD192639	2.6±1.2			20.69	a
HD206267	6.3±1.4	5.6±0.5	6.6±0.7	20.86	a
HD207198	3.8±0.5	3.9±0.4	<9.1	20.83	a
HD210121	6.2±3.2	7.6±2.4	4.2±0.5	20.75	a
HD210839	3.8±0.7	4.2±0.3	<5.7	20.84	a
HD218915	3.9±0.2			20.15	a

^aSonnentrucker et al. (2007)

^bBurgh, France, & McCandliss (2007)

^cFederman et al. (2003) and Savage et al. (1977)

^dLambert et al. (1994) and Savage et al. (1977)

Table 3. Results for Models of 2-Sided Slabs

Model	Density ^a (cm ⁻³)	G ^b	Total Extinction A_v (mag)	T_{min} (K)	$f_{max}(\text{H}_2)$ Center	$F(\text{H}_2)$ Integrated
1	50	1	1.0	82	0.92	0.79
2	100	1	1.0	62	0.96	0.89
3	200	1	1.0	46	0.98	0.94
4	100	10	1.0	138	0.75	0.46
5	200	10	1.0	122	0.87	0.64
6	100	10	0.5	164	0.37	0.22
7	100	10	2.0	92	0.95	0.71
8	199	1	0.2	106	0.74	0.62

^a $n(\text{H}) = n(\text{H}^0) + 2n(\text{H}_2)$

^bRelative to standard interstellar radiation field

Table 4. Limits on Densities for Sources Having Only J = 1–0 Data ($T^k = 100$ K)

Source	$\log(n_{min}/\text{cm}^{-3})$	$\log(n_{max}/\text{cm}^{-3})$
BD +48 3437		1.4
BD +53 2820		1.8
CPD -69 1743		1.4
HD 13268		1.8
HD 13745	1.3	2.0
HD 14434	1.6	2.1
HD 37367		1.7
HD 37903		1.4
HD 43818	1.4	2.1
HD 58510		1.5
HD 63005	0.8	1.9
HD 91983		1.4
HD 93205		1.4
HD 93222		1.8
HD 93237		1.7
HD 93840		1.7
HD 94454	1.2	2.0
HD 102065	0.8	1.9
HD 104705		2.0
HD 106943		1.4
HD 108002		1.7
HD 108639		1.6
HD 110434		1.4
HD 112999		1.6
HD 114886		1.7

Table 4—Continued

Source	$\log(n_{min}/\text{cm}^{-3})$	$\log(n_{max}/\text{cm}^{-3})$
HD 115071	1.1	1.9
HD 115455		1.5
HD 116852		1.7
HD 122879		1.5
HD 124314		1.8
HD 140037		1.5
HD 152590	1.4	2.1
HD 152723	1.3	2.0
HD 157857	1.7	2.2
HD 163758	1.3	2.0
HD 192639		1.7
HD 195965		1.6
HD 208905	2.0	2.4
HD 209481		1.5
HD 209975		1.5
HD 210809		1.7
HD 218915	1.6	1.9
HD 303308		1.7
HD 308813	1.2	2.0

Table 5. Densities¹ Derived For Sources with Excitation Temperatures for Two or Three Transitions; $T^k = 100$ K

Source	n_{min}	n_{max}	n_{min}	n_{max}	n_{min}	n_{max}	n_{min}^2	n_{max}^2
	T_{10}^{ex}		T_{21}^{ex}		T_{32}^{ex}		Combined	
CPD -59 2603		1.6	0.3	1.9	-	-	0.3	1.6
HD 12323		1.7	1.9	2.3	-	-	1.8	1.8(s)
HD 15137		1.7	1.9	2.5	-	-	1.8	1.8(s)
HD 23478		1.8	0.9	2.1	0.6	1.7	0.9	1.7
HD 24190		1.7	0.9	2.1	-	-	0.9	1.7
HD 24398		1.8	1.2	2.2	0.6	1.7	1.2	1.7
HD 24534	0.8	2.3	2.3	2.5	0.9	2.1	2.2	2.2(s)
HD 27778	1.9	2.3	2.1	2.6	0.7	2.3	2.1	2.3
HD 30122	1.2	2.0	1.4	2.2	-	-	1.4	2.0
HD 36841		1.4		1.8	-	-		1.4
HD 96675	1.1	1.9	2.6	3.0	-	-		
HD 99872	1.1	1.9	1.1	2.2	-	-	1.1	1.9
HD 137595	1.2	2.0	1.7	2.4	-	-	1.7	2.0
HD 144965	1.5	2.1	2.2	2.7	-	-	2.1	2.2(s)
HD 147683	1.9	2.3	2.5	2.9	1.6	2.8	2.4	2.4(s)
HD 147888	2.5	2.7	2.6	3.0	2.3	3.0	2.6	2.7
HD 147933		0.6	2.7	2.8	2.6	2.7		
HD 148184		1.4	2.1	2.4	0.5	3.1		
HD 148937	1.1	1.9	1.8	2.5	1.8	2.9	1.8	1.9
HD 149757	1.1	1.8	2.0	2.2	1.4	2.0	1.9	1.9(s)
HD 154368		1.6	2.0	2.6	-	-		
HD 177989		1.8		2.0	-	-		1.8
HD 185418	1.1	1.6	0.5	2.3	-	-	1.1	1.6
HD 190918		1.4	1.9	2.6	-	-		

Table 5—Continued

Source	n_{min}	n_{max}	n_{min}	n_{max}	n_{min}	n_{max}	n_{min}^2	n_{max}^2
	T_{10}^{ex}		T_{21}^{ex}		T_{32}^{ex}		Combined	
HD 192035		1.7	1.5	2.3	-	-	1.5	1.7
HD 198781		1.8	1.1	2.2	-	-	1.1	1.8
HD 203532	1.9	2.3	1.7	2.0	-	-	1.9	2.0
HD 206267	2.0	2.4	2.3	2.5	1.6	2.4	2.3	2.4
HD 207198	1.4	1.9	1.5	2.0		2.9	1.5	1.9
HD 210121	1.1	2.5	2.3	3.0	0.4	1.0		
HD 210839	1.2	1.9	1.8	2.1		1.6	1.7	1.7(s)
HD 220057		1.6	2.1	2.3	-	-		

¹Densities expressed as $\log(n(\text{H}_2))$

²(s) denotes additional 0.1 dex range in assessing consistency among various excitation temperatures

Table 6. Average Densities of Different Cloud Categories

Category	T^k (K)	$\langle n_{min} \rangle$ (cm^{-3})	$\langle n_{max} \rangle$ (cm^{-3})	$\langle n_{mid} \rangle$ (cm^{-3})
sources with T_{10}^{ex} only	100	22	105	49
sources with T_{10}^{ex} & T_{21}^{ex}	100	25	69	42
sources with T_{10}^{ex} & T_{21}^{ex}	50	32	143	67
sources with 3 T^{ex}	100	75	118	94
sources with 3 T^{ex}	50	104	176	135
sources with 2 or 3 T^{ex}	100	37	125	68
sources with 2 or 3 T^{ex}	50	58	148	92

Table 7. Excitation Temperature of Lower CO Transitions for $T^k = 100$ K, and $n(\text{H}_2) = 0.01 \text{ cm}^{-3}$ From RADEX (Van der Tak et al. 2007)

Upper Level	Lower Level	Frequency (GHz)	Excitation Temperature T^{ex} (K)	
			$T^{bg} = 0.0$ K	$T^{bg} = 2.7$ K
2	1	115.271	0.53	2.70
3	2	230.538	3.57	2.70
4	3	345.796	6.11	2.71
5	4	461.041	12.08	4.01
6	5	576.268	15.19	15.05
7	6	691.473	19.01	19.25
8	7	806.652	23.54	23.27
9	8	921.800	27.05	27.52
10	9	1036.912	30.78	30.58
11	10	1151.986	36.51	35.97
12	11	1267.015	36.90	37.69
13	12	1381.995	44.40	42.74
14	13	1496.923	40.78	42.80
15	14	1611.794	50.24	48.01
16	15	1726.603	45.42	47.24
17	16	1841.346	52.27	50.69
18	17	1956.018	49.58	51.07
19	18	2070.616	53.60	53.17
20	19	2185.135	51.45	52.19
21	20	2299.570	58.70	57.95

